Pre – Conference excursion guide

From Neoproterozoic sedimentation on the Peri-Gondwanan extended shelf to the Variscan collision of terranes. The history preserved in the Kamieniec Ząbkowicki metamorphic belt and the Doboszowice metamorphic complex

Jacek Szczepański[1], Mirosław Jastrzębski[2], Sławomir Ilnicki[3], Robert Anczkiewicz[4]

1. University of Wrocław, Institute of Geological Sciences, jacek.szczepanski@uwr.edu.pl
2. Polish Academy of Sciences, Research Centre in Wroclaw, mjast@interia.pl
3. University of Warsaw, Department of Geochemistry, Mineralogy and Petrology, slawomir.ilnicki@uw.edu.pl
4. Polish Academy of Sciences, Research Centre in Kraków, ndaczki@cyfronet.pl

The field trip is focused on rock successions exposed in the Kamieniec Metamorphic Belt (KMB) and the Doboszowice Metamorphic Complex (DMC) located in the Fore-Sudetic Block at the NE margin of the Bohemian Massif (Fig. 1). Here, the crystalline basement forms small and isolated outcrops, emerging only in places from the overlying Cenozoic cover. This part of the Bohemian Massif is located at the eastern extremity of the Central European Variscides that exposes three major units from west to east: 1) the Teplá-Barrandian Unit consisting of Neoproterozoic basement and its Early Palaeozoic cover that according to some authors is exposed in the Góry Sowie Block (GSB); 2) the Saxothuringian Unit that is exposed both west of the GSB in the Karkonosze-Izera Massif and east of the GSB in the KMB and the DMC; and 3) the Brunovistulian Neoproterozoic basement with Early to Late Palaeozoic cover that is exposed in the East Sudetes represented by the Strzelin Crystalline Massif and the Jeseniky Mts. Generally, metamorphic complexes of the Bohemian Massif have recently been interpreted as the result of a long-lasting Andean-type convergence and collision of the Saxothuringian, Teplá-Barrandian and Brunovistulian Units of the Central European Variscides (e.g. Schulmann et al. 2009; Mazur et al., 2010; Chopin et al., 2012).

The aim of the pre-conference field trip is to present the latest data and interpretations on the provenance of the detrital material, its maximum depositional age and the tectonic setting of deposition, as well as the structural and metamorphic evolution of the KMC and DMC within the framework of the Central European Variscides.

The KMB forms c. 25 km long and 5 km wide longitudinal belt between the Góry Sowie Massif and the Niemcza Shear Zone in the west and the Strzelin Crystalline Massif (including the Lipowe Hills) in the east (Fig. 1). A volcano-sedimentary succession exposed in the KMB is dominated by mica schists (stops 1 and 2) intercalated with scarce paragneisses, marbles, quartz-graphite schists, eclogites (stop 2) and felsic metavolcanics (stop 1, Fig. 2). The latter are interpreted as tuffs or lava flows (Dziedzicowa, 1966) or sills (Szczepański et al., 2023). On the contrary, the DMC is a c. 6 km long exposure of crystalline basement located south-east of the KMB and directly west of the Niedźwiedź Amphibolite Massif (NAM, Fig. 1). The DMC may be divided into western and eastern parts (Fig. 2). The western part exposes the Doboszowice orthogneiss

with Cambro-Ordovician protolith age (stop 3). The eastern part is mainly composed of the migmatic Chałupki paragneiss (stop 4) interleaved with scarce mica schists and metabasalts of unknown age.

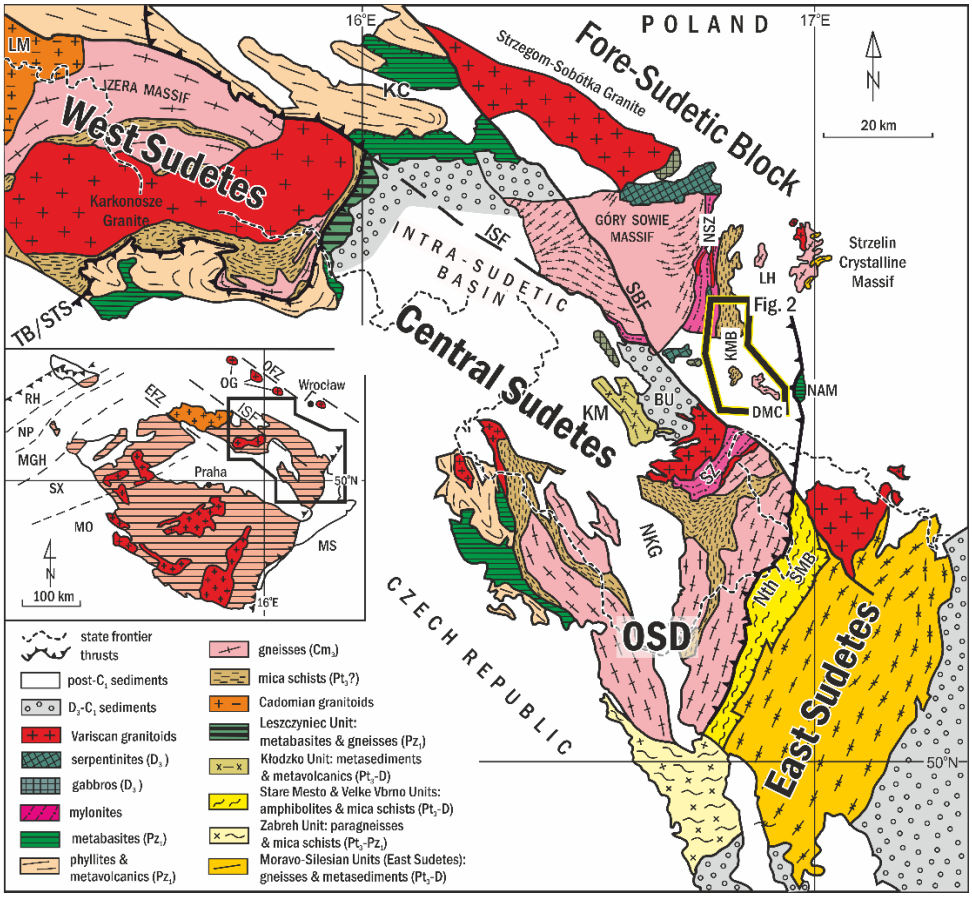

Fig. 1. Geological sketch map of the Sudetes after Mazur et al. (2006). Abbreviations: BU — Bardo Unit; KC – Kaczawa Complex; KM — Kłodzko massif; KMB – Kamieniec Metamorphic Belt; DMC – Doboszowice Metamorphic Complex; LM — Lusatian massif; NKG – Nysa Kłodzka Graben, NAM — Niedźwiedź Massif; NSZ – Niemcza Shear Zone; LH – Lipowe Hills Massif; OSD —Orlica-Śnieżnik Dome; SMB— Staré Město Belt. Sutures and faults: ISF — Intra-Sudetic fault; Nth – Nyznerov thrust; SBF — Sudetic boundary fault; TB/STS — Teplá-Barrandian/Saxothuringian suture. Abbreviations in inset: EFZ – Elbe Fault Zone, MGH — Mid-German Crystalline High; MO — Moldanubian zone; MS — Moravo-Silesian zone; NP — Northern Phyllite zone; OG – Odra granitoids, OFZ – Odra Fault Zone, RH — Rhenohercynian zone; SX — Saxothuringian zone. Age assignments: Pt — Proterozoic; Pz — Palaeozoic; Cm — Cambrian; Or — Ordovician; D — Devonian; C — Carboniferous; 1 — Early; 2 — Middle.

Age and provenance of rock successions

The protolith age of the volcano-sedimentary successions exposed in the KMB and DMC is poorly known. The available data suggest that the maximum depositional age (MDA) of the KMB and the adjacent Lipowe Hills mica schists is in the range of c. 560-570 Ma (Neoproterozoic, Oberc-Dziedzic et al., 2018; Jastrzębski et al., 2020), while the Chałupki paragneiss from the DMC has a late Cambrian MDA (Jastrzębski et al., 2023). However, Szczepański et al. (2023) argue that the mica schist from the KMB displays the MDA at 529 Ma (early Cambrian), whereas the paragneiss from the DMC displays the MDA at 456 Ma (Upper Ordovician).

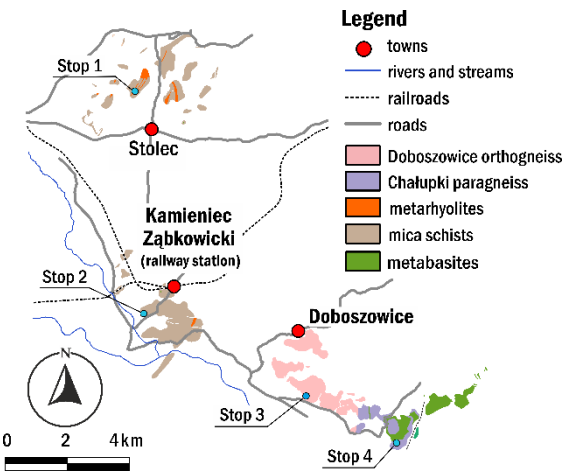

Fig. 2. Geological sketch map of the southern part of the Kamieniec Metamorphic Belt and the Doboszowice Metamorphic Complex.

Consequently, the published zircon age spectra suggest that the studied volcano-sedimentary successions exposed in the eastern part of the Fore-Sudetic Block may represent two different rock sequences in terms of MDA. In addition, a sedimentary succession of the KMB was injected by several rhyolitic sills. Interpretation of the metarhyolites as sills is supported by their very consistent chemical composition and textural features, with no evidence of e.g. degassing. The zircons from the KMB metarhyolites are dominated by an age peak of 510 Ma that is interpreted as the time of magmatic emplacement. Rare Neoproterozoic and Archaean inheritance points to the involvement of an older crustal component in magma genesis.

Based on the trace element composition, the metasedimentary successions from the KMB and DMC are interpreted to be derived from a felsic source and their chemical composition was not significantly affected by alteration during transport (Fig. 3).

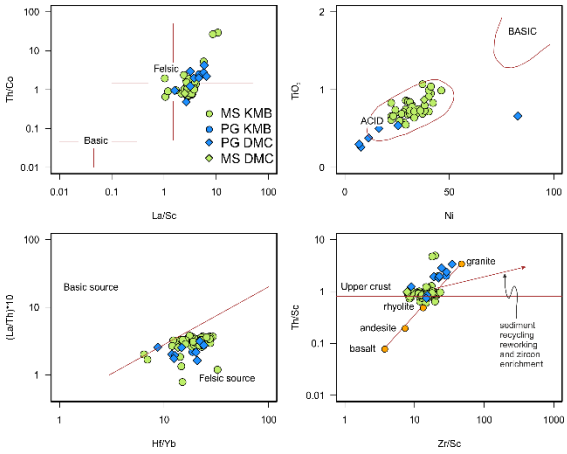

Fig. 3. Diagrams illustrating lithology of the source area after (a) Cullers (2002), (b) Floyd, Winchester & Park (1989), (c) Hladil et al. (2003), and (d) the influence of sediment recycling and zircon enrichment on chemical composition of the investigated quartzites after McLennan et al. (1993). MS – mica schists, PG – paragneisses.

Furthermore, the chemical composition of the mica schists and paragneisses from the KMB and DMC is typical of sediments derived from erosion of suprasubduction complexes (Fig. 4).

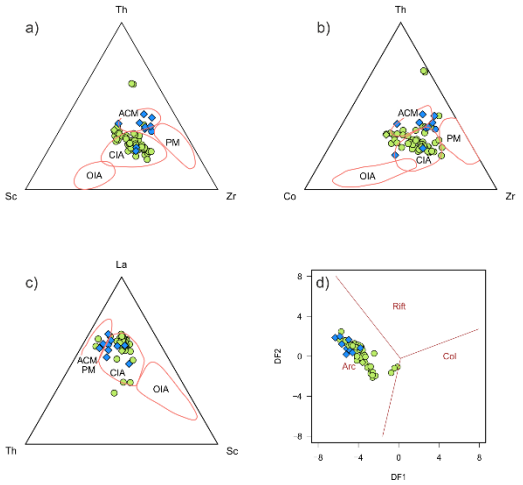

Fig. 4. a-c) Discrimination diagrams showing tectonic setting of deposition of the protolith to the mica schists and paragneisses of the Kamieniec Metamorphic Belt and the Doboszowice Metamorphic Complex. After Bhatia & Crook (1986). Abbreviations: PM – passive margin, CIA – continental island arc, ACM – Active continental margin, OIA - oceanic island arc. d) discriminant-function multi-dimensional diagram after Verma & Armstrong-Altrin (2013). Abbreviations: Arc – arc related setting, Rift – continental rift setting, Col – collisional setting. Samples fall in the field typical of arc-related sediments. Symbols as in Fig. 3.

Available detrital zircon ages from Cambro-Ordovician sedimentary successions covering the Saxothuringian and Teplá-Barrandian Units exposed in the Sudetes clearly indicate that all these Neoproterozoic crustal fragments were derived from the same cratonic areas and Cadomian arc-related basement (Fig. 5) located at the northern periphery of Gondwana, close to the West African Craton or Trans-Saharan Belt (Fig. 6; corresponding references are given on Fig. 6).

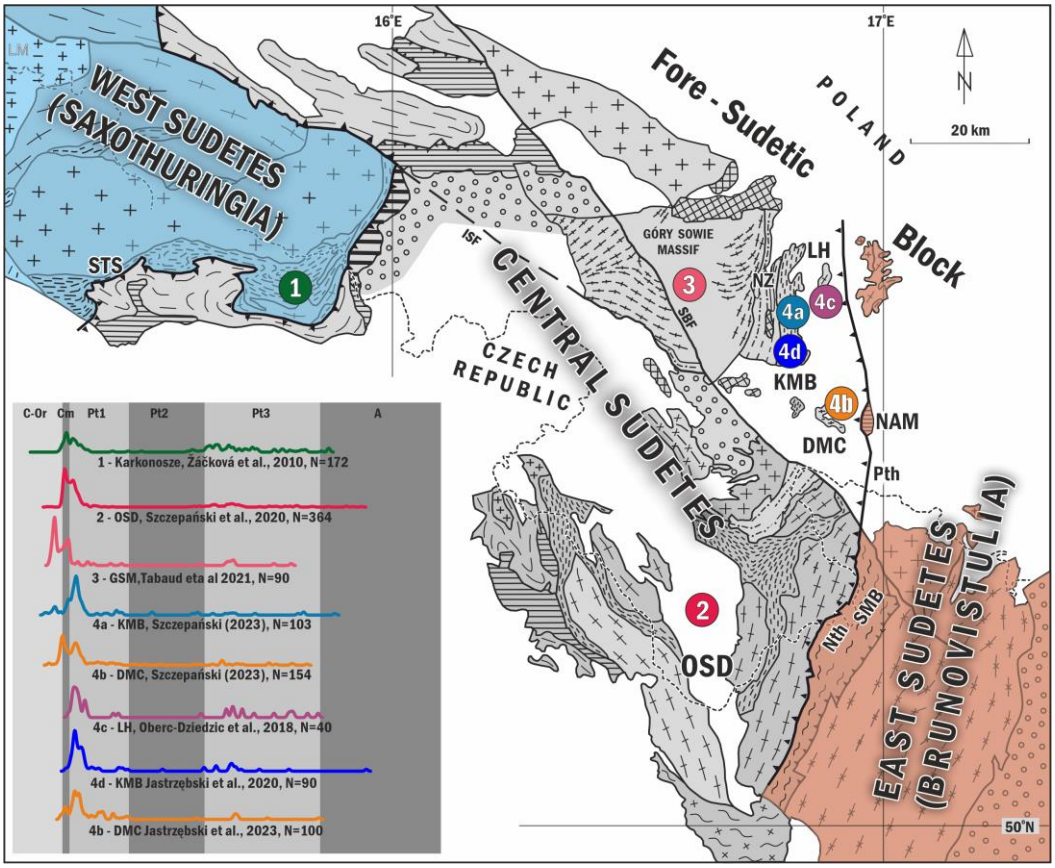

Fig. 5. Comparison of zircon age spectra obtained for various crustal domains from the Sudetes shown on the geological sketch map of the Sudetes after Mazur et al. (2006). Kernel density plots for detrital zircons from: 1. Karkonosze (Žáčková et al., 2010), 2. Orlica-Śnieżnik Dome ; 3. Góry Sowie Massif (Szczepański et al., 2020; Tabaud et al., 2021)**; 4a. Kamieniec Metamorphic Belt (Szczepański et al., 2023), 4b – Doboszowice Crystalline Massif (Szczepański et al., 2023; Jastrzębski et al., 2023), 4c – Lipowe Hills (Oberc-Dziedzic et al., 2018); 4d – Kamieniec Metamorphic Belt (Jastrzębski et al., 2020); 5. Brunovistulia (Friedl et al., 2004; Mazur et al., 2010), 6. Staré Město Belt (Śliwiński et al., 2022). Abbreviations: STS – Saxothuringian suture, OSD – Orlica-Śnieżnik Dome, DMC – Doboszowice Crystalline Massif, KMB – Kamieniec Metamorphic Belt, NZ – Niemcza Zone, LH – Lipowe Hills, NAM – Niedźwiedź amphibolite Massif, Pth – Paczków thrust, Nth – Nyznerov thrust, SMB – Staré Město Belt. Abbreviations in inset: C-Or – Carboniferous-Ordovician, Cm – Cambrian, Pt1 – Neoproterozoic, Pt2 – Mesoproterozoic, Pt2 – Paleoproterozoic, A – Archean. Abreviations: Ph – Phanerozoic, Pt1 – Neoproterozoic, Pt2 – Mesoproterozoic, Pt2 – Paleoproterozoic, A – Archean.**

Consequently, we support suggestions that during the Cambro-Ordovician time Cadomian crustal fragments now exposed in the western and central parts of the Fore-Sudetic Block were dispersed along the northern periphery of Gondwana, most probably forming an extended shelf that developed on a passive continental margin (Fig. 6; e.g. Drost et al., 2011; Žák and Sláma 2018; Collett et al., 2021; Tabaud et al., 2021; Collett et al., 2022).

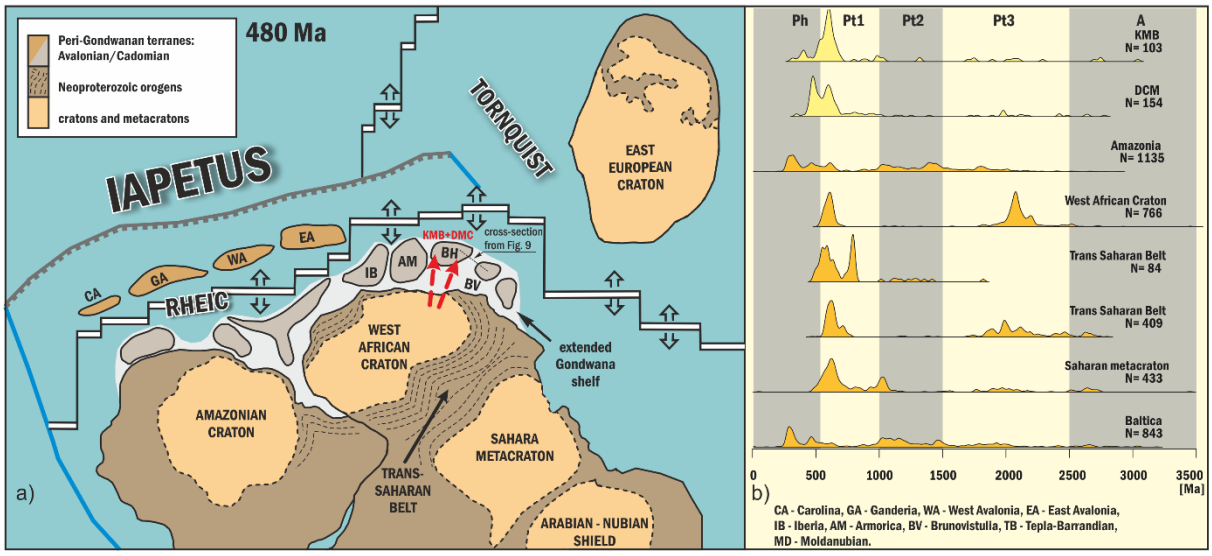

Fig. 6. a) Tentative simplified reconstruction of Western Gondwana extended passive margin during the Early Ordovician, modified after (Domeier, 2016) and (Torsvik, 2017). Abbreviations: CA – Carolina, GA – Ganderia, WA – West Avalonia, EA – East Avalonia, IB – Iberia, AM – Armorica, BV – Brunovistulia, BH – Saxothuringia, Tepla-Barrandian and – Moldanubia, KMB – Kamieniec Metamorphic Belt, DMC – Doboszowice Metamorphic Complex. Red arrows indicate the main directon of sedimentary transport. Types of lithospheric boundaries: black-white – spreading ridge, grey – subduction, blue – transform. b) Kernel density plots for detrital zircons from: Kamieniec Metamorphic Belt (Szczepański et al., 2023), Doboszowice Metamorphic Complex (Szczepański et al., 2023), Amazonian Craton (Gaucher et al., 2008; Geraldes et al., 2014; Pankhurst et al., 2016, West African Craton (Abati et al., 2010), Trans-Saharan Belt – Tuareg Shield (Henry et al., 2009), Trans-Saharan Belt (Peucat et al., 2003; Abdallah et al., 2007; Bendaoud et al., 2008; Bosch et al., 2016), Saharan Metacraton (Meinhold et al., 2011) and Baltica (Valverde-Vaquero et al., 2000; Kristoffersen et al., 2014; Kuznetsov et al., 2014). Kernel density plots were designed via the R software environment (R Core Team, 2012).

Age of tectonothermal events

The volcano-sedimentary successions comprised in the KMB and DMC suffered a Variscan metamorphism and deformation. According to several authors, it was related to continental collision between Gondwana-derived crustal domains represented by the Teplá-Barrandian, Saxothuringian and Brunovistulian domains (e.g. Schulmann et al., 2009; Chopin et al., 2012; Jastrzębski et al., 2020; Szczepański et al., 2022; Szczepański & Goleń, 2022).

Time constraints on the age of metamorphism and the related deformation in this part of the Fore-Sudetic Block have been supplied by ^{40}Ar-^{39}Ar geochronology on hornblende, yielding two distinct ages of 331.9±1.7 Ma and 376 Ma for hornblende-bearing rocks from the Niemcza Shear Zone (NSZ in Fig. 1) and the KMB, respectively (Steltenpohl et al., 1993). The volcano-sedimentary succession of the Kamieniec Metamorphic Belt was also intruded by syn- to post-tectonic granodiorites dated at 330–340 Ma by U-Pb and Pb-Pb methods on zircons (Oliver et al., 1993; Kröner and Hegner, 1998). Furthermore, ages in the range of 380 and 330 Ma were obtained using U-Pb and Pb-Pb method on zircons from syntectonic diorites and monzodiorites from the adjacent Niemcza Shear Zone (Pietranik et al. 2013; Pietranik and Majka 2017). The age of the tectonothermal event recorded in the KMB has recently been estimated at c. 330 Ma (Jastrzębski et al., 2020) and in the DMC at c. 346–341 Ma based on ICP–MS U–Th–Pb dating of monazite (Jastrzębski et al., 2023). Variscan age of tectonothermal event

is confirmed by the youngest single zircon grains documented in the metasediment samples from the KMB and DMC showing ages of c. 330-320 Ma that are interpreted as reflecting lead loss owing to the Variscan thermal overprint (Szczepański et al., 2023). This is in agreement with Lu–Hf and Sm–Nd garnet dating of the Chałupki paragneiss, which shows that these rocks were metamorphosed between c. 347 Ma and c. 337 Ma (Szczepański et al., 2022). Consequently, the time frame for Variscan tectono-thermal activity in this area covers the time span from c. 380 Ma to c. 330 Ma.

Deformation and metamorphism

Three main ductile deformation events: D1 to D3, were documented in the KMB and DMC. Generally, rocks of the DMC preserve relics of older deformation events (D1 and D2), whereas the mica schists of the KMB usually contain structures of all the documented deformation events (D1 to D3).

D1 structures

The oldest, D1, structures comprise the S1 foliation which is mostly sub-vertical in the KMB and sub-horizontal in the paragneisses of the DCM (Fig. 7). It was documented as either mesoscopic, penetrative planar structures observed in the field (Fig. 8a, c and f), relic structures preserved in microlithons between younger cleavage planes or as inclusion trails conserved within inner parts of garnet porphyroblasts (Fig. 8b and e). The S1 planes observed in the field and preserved in rocks of the KMB display no signs of clear metamorphic differentiation. Particular layers show variable thickness and are oriented parallel to lithologic boundaries (Fig. 8a), suggesting that the S1 may be parallel to bedding. In the KMB the S1 schistosity generally dips at high angles towards SE or NW (Fig. 7a). However, in places in the KMB and in the DMC the S1 foliation shows a nearly horizontal orientation or dips at shallow angles towards the NW or SE in the normal limbs of younger F2 folds (Fig. 7a and e). The original orientation of the S1 foliation is unknown because it is scattered along a great circle due to the F2 folding (Fig. 7a, e and f). In strongly deformed portions of the mica schists of the KMB, the only relics of the S1 foliation are inclusion trails conserved mostly in garnet porphyroblasts (Fig. 8b and e). These inclusion trails are rectilinear or, occasionally, folded (Fig. 8b and e) and comprise mainly rutile, quartz, white mica and chloritoid. The S1 planes preserved in the Chałupki paragneiss are marked by migmatitic laminae that contains the L1 mineral lineation oriented E-W (Fig. 7e). In rock sections parallel to this lineation and perpendicular to the S1 planes a set of kinematic indicators including sigma type feldspar porphyroclasts was documented. All these kinematic indicators point to top-to-E sense of non-coaxial shear during the D1 event (Fig. 8c).

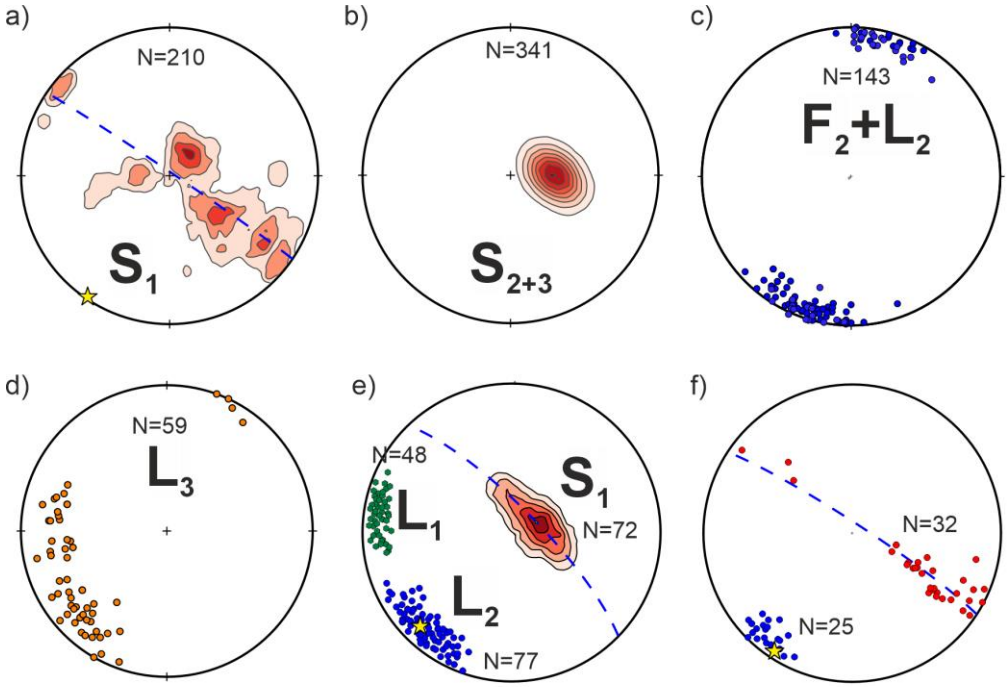

Fig. 7. Equal-area lower hemisphere projections showing: (a) scatter of mostly steep S1 foliation in the KMB, yellow star - axis of great-circle girdle of foliation, blue dashed line - great-circle girdle of foliation, (b) orientation of S2+3 planes in the KMB, (c) orientation of F2 folds and L2 lineation in the KMB, (d) orientation of L3 mineral lineation in the KMB, (e) contour lines - scatter of mostly subhorizontal S1 foliation in the Chałupki paragneiss of the DMC, yellow star - axis of great-circle girdle of foliation, blue dashed line - great-circle girdle of foliation, green points are for L1 mineral lineation, blue points are for L2 mineral lineation, (f) red points are for S1 foliation in the Doboszowice orthogneiss of the DMC, yellow star - axis of great-circle girdle of S1 foliation, blue dashed line - great-circle girdle of foliation, blue points are for L2 mineral lineation.

D2 structures

The D2 structures are represented by the F2 folds, the subhorizontal S2 axial planar cleavage and the L2 lineation. The scale of the F2 folds grades from open, several meter- through centimetre- to millimetre-scale asymmetric structures with their axes trending NNE-SSW (Fig. 7c). In many outcrops, rootless isoclinal folds have been documented in NE-SW oriented cross-sections, which we interpret as sections through the F2 folds that are slightly oblique to their axes. Therefore, the commonly observed elongated quartz lenses may represent hinges or limbs of the F2 folds. The subhorizontal S2 cleavage developed parallel to the axial planes of the F2 folds (Fig. 8d). The newly formed S2 planes dip towards the WSW to W at moderate to shallow angles (Fig. 7b). The S2 planes represent a cleavage in those places where the F2 folds are of considerable size and mica schists are intercalated with abundant quartzofeldspathic schists. Elsewhere, the S2 planes define mostly a penetrative foliation. Garnet grains, usually reaching 5–8 mm and, sporadically, even 30 mm in diameter, are often characterized by the occurrence of rectilinear or folded inclusion trails (Fig. 8b and e). The F2 folding resulted in the scatter of the S1 foliation along a great circle with a subhorizontal axis extending in the NNE-SSW direction (Fig. 7a, e and f). Lineation developed parallel to the F2 axes is preserved on the S1 and S2 planes, striking generally NNE-SSW to NE-SW (Fig. 7c, e and f). In places, the mineral lineation L2m is defined by

parallel alignment of white mica flakes, and, locally, an intersection lineation L2i formed by intersection of the S1 and S2 planes. On the contrary no signs of the L1 lineation was documented in rocks of the KMB.

D3 structures

The D3 deformation resulted in reactivation of the older S2 planes and led to the formation of the composite S2+3 planar structures that vary in their frequency of occurrence. The S2+3 foliation dips at moderate to shallow angles towards the W (Fig. 7b). Locally, a NE-SW to nearly E-W trending L3 mineral lineation on the S2+3 planes is preserved, being defined by parallel alignment of mica flakes (Fig. 7d). The orientation of the L3 mineral lineation changes from NE-SW, where the S2+3 planes are non-penetrative, to nearly E-W, where the S2+3 foliation becomes penetrative. The rock sections perpendicular to the S2+3 planes and parallel to the L3 mineral lineation reveal such kinematic indicators as S-C structures, sigma type porphyroblasts, extensional crenulation cleavage and sigmoidal inclusion trails. All these indicators document a top-to-SW or top-to-W sense of non-coaxial shear related to the D3 deformation (Fig. 8g and h). The domains with preserved asymmetric D3 fabric are sometimes filled with granitic material forming ~10–25 cm long lenses aligned parallel to the main S2+3 foliation. Sigmoidal inclusion trails conserved in garnet grains, plagioclase and andalusite porphyroblasts suggest synkinematic growth of these minerals during the D3 event (Fig. 8h). Furthermore, staurolite grains aligned mostly parallel to the main S2+3 foliation indicate syn-D3 growth.

Mineral assemblages stable during deformation

In the KMB the deformation events D1 to D3 are characterized by two different sets of stable mineral assemblages M1 and M2. The M1 assemblage coexisted during the D1 and the beginning of the D2 deformation events, whereas the assemblage M2 was stable at least during the terminal phase of the D2 event and the entire D3 deformation. The proposed assignment of mineral assemblages to particular deformation events is mainly based on garnet porphyroblasts displaying diverse inclusion sets with strikingly different geometry, which implies that two generations of garnets are preserved. The first garnet generation (Grt1) contains mostly chloritoid and rutile inclusions that are sporadically accompanied by chlorite and pseudomorphs after lawsonite. These inclusion sets in some porphyroblasts are developed as rectilinear, while in others as folded inclusion trails (Fig. 8b and e). The second garnet generation (Grt2) displays mostly sigmoidal ilmenite inclusions (Fig. 8h) accompanied by staurolite, plagioclase and biotite. In some samples both types of complex garnet porphyroblasts occur (Grt1 and Grt2, Fig. 8b). In such porphyroblasts inclusion trails display strikingly different orientation and composition of Ti-rich mineral phases (rutile in Grt1 and ilmenite in Grt2). Consequently, ilmenite in Grt2 points to garnet growth at P–T conditions related to exhumation (Cao et al. 2021; Szczepański et al. 2021). Importantly, the ilmenite inclusions preserved in Grt2 extend into the rock matrix. As suggested by the geometry of the observed inclusion trails, grading from rectilinear to slightly folded, the Grt1 must have started to grow during the D1 and likely continued through to the initial phases of the D2 event. The Grt2 crystallized synkinematically with respect to the D3 non-coaxial

shearing. Importantly, the KMB mica schists are characterized by the occurrence of two groups of white mica that differ significantly in Si content. The Ms1 mica displays phengitic composition with up to 3.40 Si apfu, while the Ms2 white mica shows muscovite composition with up to 3.20 Si apfu.

The calculated P–T conditions for the early stage of metamorphism and related deformation (M_1 and D_1) in the KMB are at c. 485±25°C and 18±1.8 kbar. Subsequently, the D_3-M_2 events underwent at P–T conditions ranging from 520±26°C and 6±0.6 kbar through 555±28°C and 7 kbar±0.7 to ~590±30°C and 3–4±0.4 kbar.

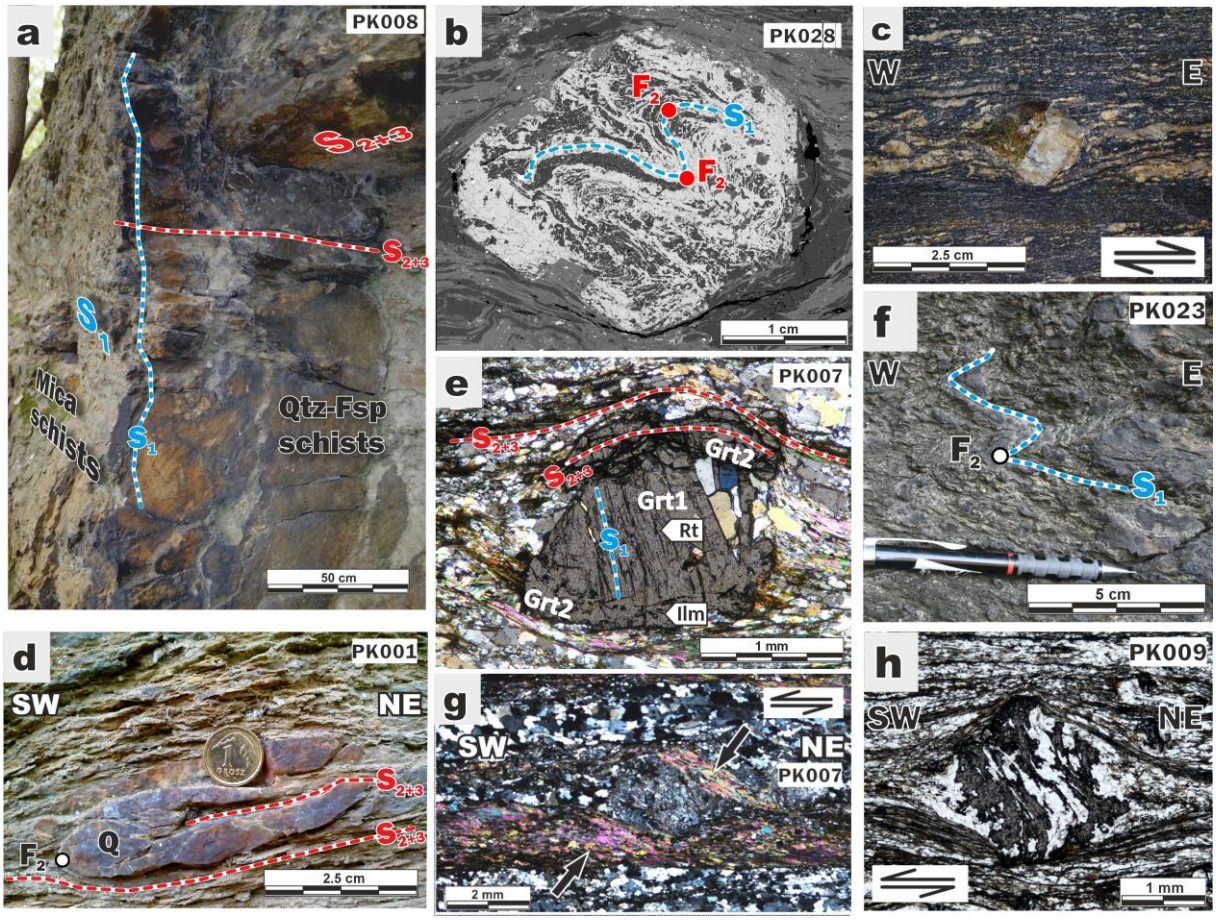

Fig. 8. (a) Field photographs documenting steep older S1 fabric (blue dashed line) oriented parallel to the lithological boundary and in places overprinted by non-penetrative shallow S2+3 planes (red dashed line), KMB mica schist, (b) photomicrograph showing S_1 planes refolded into F_2 folds preserved in garnet porphyroblast in the KMB mica schist, (c) sigma-type feldspar porphyroclast in the Chałupki paragneiss documenting top-to-E kinematics of D_1 event, (d) F_2 isoclinal fold in the KMB mica schist, (e) complex garnet porphyroblast; preserved in its inner part inclusion trails define S_1 planes (early garnet generation – Grt1), and S_2 planes conserved in its rim part continue into the matrix of the rock (late garnet generation – Grt2), the KMB mica schist, (f) cm-scale F_2 folds in mica schists from the KMB, (g) asymmetric pressure shadows filled with quartz and deformation mats (arrows) filled with white mica developed around plagioclase porphyroblast documenting top-to-SW kinematics of D_3 event, (h) sigmoidal inclusion trails preserved in Grt2 documenting top-to-SW kinematics of the D_3 event.

The paragneiss from the DMC is characterized by two mineral assemblages that originated during prograde metamorphism and resulted from two distinct metamorphic events M1 and M2. The younger and well-preserved HT–MP paragenesis M2 overgrowing the older and poorly preserved

HP–LT mineral assemblage M1. The M1 paragenesis comprises scarcely preserved phengitic white mica with Si contents reaching up to 3.38 apfu and forming cores of white mica grains and relics of rutile grains preserved in abundant ilmenite crystals. Both equilibrium modelling and conventional geothermobarometry are inconclusive but suggest pressures of ca. 12–18 kbar at temperatures of c. 500–570°C for the M1 event. In contrast, the younger and well-preserved the M2 paragenesis contains abundant K-white mica with low Si content (< 3.15 apfu) accompanied by garnet, plagioclase, staurolite, kyanite and ilmenite. The HT–MP nature of the M2 event is supported by P–T modelling of garnet growth, indicating a progression of P and T during garnet growth and a maximum pressure and temperature of its formation of c. 660°C at 9 kbar.

Towards a new tectonometamorphic model

Recently, Szczepański and Goleń (2022) proposed a new tectonometamorphic model of the evolution of the eastern part of the Fore-Sudetic Block during the Variscan orogeny. They interpreted the M1 and D1 events as a result of subduction of the protolith of mica- and quartzofeldspatic schists of the KMB to depth of ~65–70 km in relation to the collision between the Saxothuringian and Brunovistulian terranes. This was followed by exhumation to mid-crustal level (of ~20–25 km) during the D2 event. Subsequently, the D3-M2 events show evidence of non-coaxial flow of possibly overthickened, hot and mechanically unstable orogenic crust at mid-crustal level. We postulate that the granitoid magmatism occurring at this stage of the KMB evolution may have been responsible for mechanical weakening of an overthickened nappe pile, thus facilitating reactivation of the already existing foliation and enabling the second stage of exhumation (D3 event).

According to Mazur and Józefiak (1999), the KMB, together with the adjacent DMC, comprises three refolded tectonic units interpreted as fragments of crystalline nappes with different metamorphic records. The base of the refolded nappe pile is defined by the Paczków thrust, which separates it from the underlying metabasites of the Niedźwiedź Massif (Pth in Fig. 1, Mazur and Józefiak 1999). It is believed that the Paczków thrust represents a northern continuation of the Nýznerov thrust, separating the metamorphic complexes of the Central and East Sudetes (Fig. 1; Skacel, 1989).

According to Mazur and Józefiak (1999), the nappe stacking (D1) and folding (D2) of the whole nappe pile was related to east-west directed shortening that had resulted from a collision between crustal domains that are now interpreted to correspond to the Brunovistulian (East Sudetes) and Saxothuringian (Central Sudetes) terranes (e.g. Mazur et al., 2015). During the terminal stage of the evolution of the KMB, the overthickened and mechanically unstable nappe pile was affected by a SW-directed gravitational collapse, producing low-angle normal-slip shear zones (D3). The data presented by Szczepański et al. (2022) and Szczepański and Goleń (2022) on the described tectonometamorphic events are, to some degree, in agreement with the tectonic model proposed by Mazur and Józefiak (1999) for the evolution of the KMB. According to this model, the volcano-sedimentary succession of the Kamieniec Metamorphic Belt was affected by east-vergent folds formed in response to the Variscan collision between the Saxothuringian and Brunovistulian terranes. Data presented by Szczepański and Goleń (2022) reinforces this model and shows that the

regional-scale folding can be interpreted as coeval with the first stage of the exhumation of the entire KMB to a mid-crustal level (D2 event). The important difference between models proposed by Szczepański and Goleń (2022) and Mazur and Józefiak (1999) is the discovery of HP–LT metamorphic record, which allow to identify that folding of the KMB succession was related to exhumation within the collision zone from depths corresponding to ~18 kbar.

It is interesting to note the difference in temperature of the M2 metamorphic event recorded in rock complexes of the DMC and KMB. The difference is c. 70–80°C and is, therefore, beyond the error of the methods used to reconstruct the P–T conditions of metamorphism in both units. This is consistent with the observed migmatization in the DMC and its absence in the KMB, although, the rock successions of the DMC are located only 3 km SE of the KMB. Furthermore, temperatures of metamorphism increase towards the E in the direction of the NAM, which is located directly east of the DMC, where they reach max. 790°C (Puziewicz and Koepke 2001; Awdankiewicz 2008). This implies a very steep geothermal gradient during the M2 metamorphism, precluding heating by large-scale processes such as thickening, shearing and thermal relaxation. It seems that the most plausible explanation for the higher temperatures of the M2 event in the DMC is related to local heat source caused by a nearby and relatively small granitoid intrusion. Such an intrusion can be exemplified by the Staré Město granitoid. Although, the above mentioned granitoid to the NE of the Sudetic Boundary Fault and are not exposed on the surface, it is highly probable that they continue within the border zone between Brunovistulia and Saxothuringia towards the NAM. This view is supported by similar metamorphic records preserved both in the rocks of the NAM and the Staré Město Belt, manifested by incipient melting preserved in the rocks of both units which occurred at c. 770–790°C and 12–13 kbar (Parry et al. 1997; Puziewicz and Koepke 2001; Awdankiewicz 2008; Jastrzębski 2012). Furthermore, the episodes associated with granitoid emplacement ranging in age from 344 to 336 correlate well with the time of garnet formation in the DMC and KMB mica schists reported in the next section (Parry et al. 1997; Štípska et al. 2004; Jastrzębski 2012; Skrzypek et al. 2014).

Chronology and dynamics of Variscan collision between Saxothuringia and Brunovistulia recorded by metamorphic successions of the DMC and KMB

The available data allow to propose a time-frame for the events related to the Variscan collision of Saxothuringia and Brunovistulia, now exposed in the eastern part of the Fore-Sudetic Block. This includes the burial of volcano-sedimentary successions of the KMB and DMC within the subduction zone followed by their exhumation in front of the rigid Brunovistulian crustal domain. Exhumation of the KMB and DMC rock successions was associated with folding, which is best documented in mica schists exposed in the KMB (Szczepański et al. 2022; Szczepański and Goleń 2022). The described scenario is similar to that proposed for the Orlica-Śnieżnik dome, located in the Central Sudetes, i.e. to the south of the KMB and DMC, and described by Chopin et al. (2012) and Mazur et al. (2012). The model invoking eastward subduction is supported by the occurrence of Devonian metamorphosed suprasubduction basic and intermediate volcanics, documented in the Brunovistulian basement and dated at c. 371 Ma

(Janoušek et al. 2014), and Devonian quartzites of the Jegłowa Beds with supra-subduction characteristics, outcropping in the Strzelin Massif (Szczepański 2007).

The latter massif is interpreted as a part of the crystalline basement of the Brunovistulian terrane exposed on the Fore-Sudetic Block (Oberc-Dziedzic et al. 2003). Consequently, the described metamorphosed Devonian metavolcanics and quartz-rich sediments with suprasubduction characteristics resulted from the oceanic subduction stage preceding the collision between Saxothuringia and Brunovistulia. The time of closure of the oceanic domain between Saxothuringia and Brunovistulia, resulting in continental collision, is most likely recorded by the core of garnet grains from mica schist sample collected in the KMB, dated at 344.6±1.1 Ma by the Lu–Hf method. These garnet grains bear a well-preserved record of HP–LT metamorphism (Szczepański et al., 2022). Furthermore, garnets form this sample contain thin rims produced during the MP–MT event (Szczepański et al., 2022). Therefore, we interpret the obtained Lu–Hf age of garnet from this sample as approximately the age of the HP–LT event. Consequently, the transition from oceanic subduction stage to continental collision took c. 27 Ma and occurred between c. 371 and c. 344 Ma. Interestingly, the same age within error of 345.5±5.0 Ma was also obtained for the garnet core from paragneiss sample from the DMC. However, according to mineral equilibria modelling this garnet started to grow at pressure of 4 kbar, which is considerably lower compared to this recorded by the garnet core from mica schists sample collected in the KMB. A similar within error Lu–Hf age of 346.9±3.6 Ma was also obtained for the whole garnet from paragneiss sample from DCM. This suggests that the exhumation from depth corresponding to 18 kbar to shallow crustal level equivalent to 4 kbar was most probably a relatively fast process. On the other hand, the thermal peak of the M2 metamorphism suffered by the rocks of the DMC is most probably recorded by the Sm–Nd garnet rim dating from paragneiss sample delivering an age of 337.3±6.6 Ma. Therefore, the growth of garnet in sample MD01-18 corresponding to the M2 episode took place in the time interval between 345.5 Ma and 337.3 Ma giving c. 8.2 Ma. This time interval fits quite well with the time of granitoid intrusions penetrating the Staré Město Belt and possibly also the NAM.

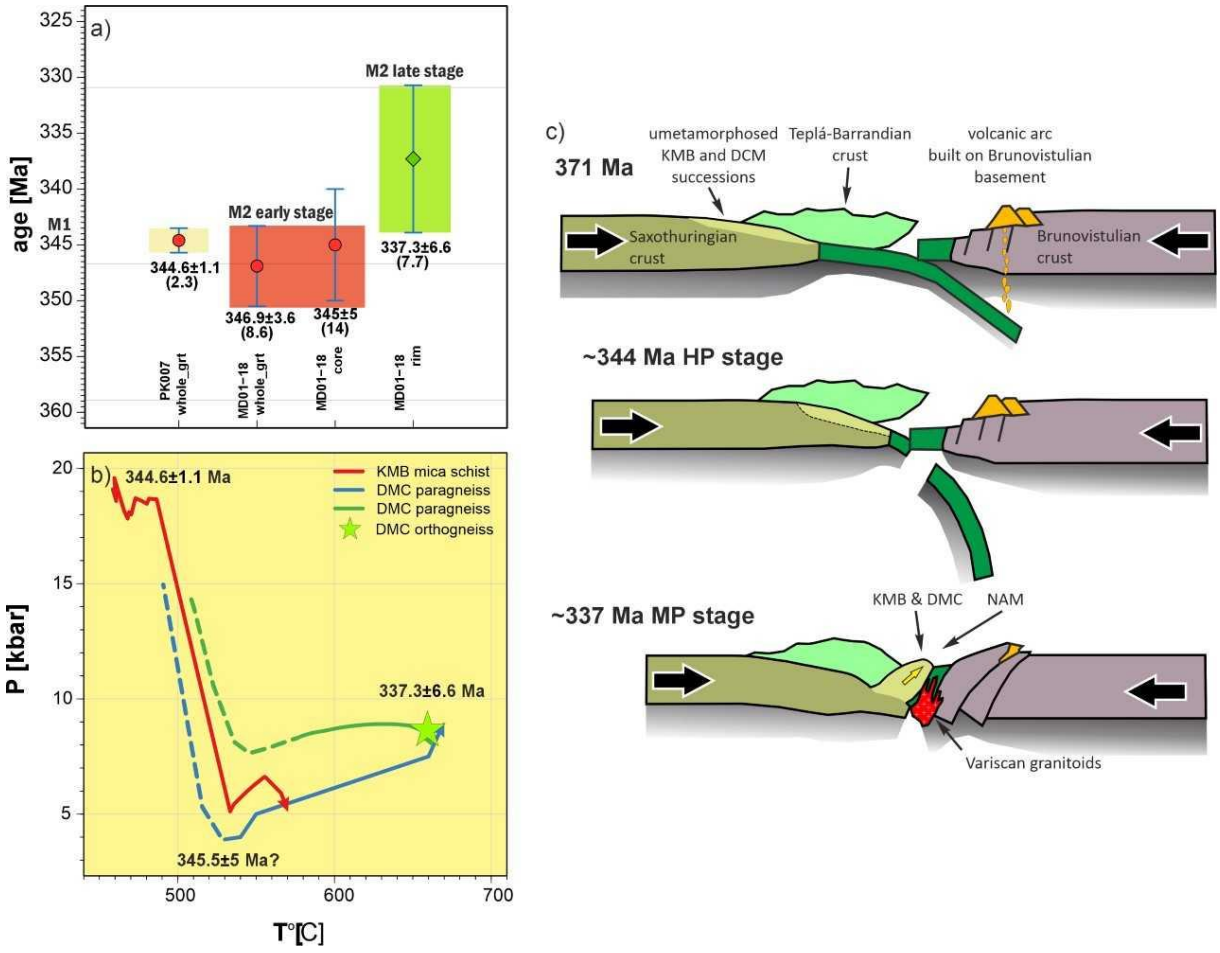

Fig. 9. (a) summary of garnet dating using Lu–Hf (red circles) and Sm–Nd (green diamonds) methods; whole grt is for whole garnet dating, core and rim is for core and rim dating, respectively; error bars are shown with blue lines; (b) Summary of inferred P–T paths calculated for the investigated samples. The solid lines mark the part of the P–T path reconstructed based on garnet composition, while dashed lines mark the P–T path portions reconstructed based on other minerals (mainly white mica composition); green star is for thermal peak of the M2 metamorphism responsible for garnet growth in sample MD09-02; dates are based on Lu–Hf and Sm–Nd garnet dating presented in Fig. 9a. (c) Tectonic model (not to scale) showing a possible mechanism of burial and exhumation of the DMC and KMB successions.

Stop 1 – Stolec

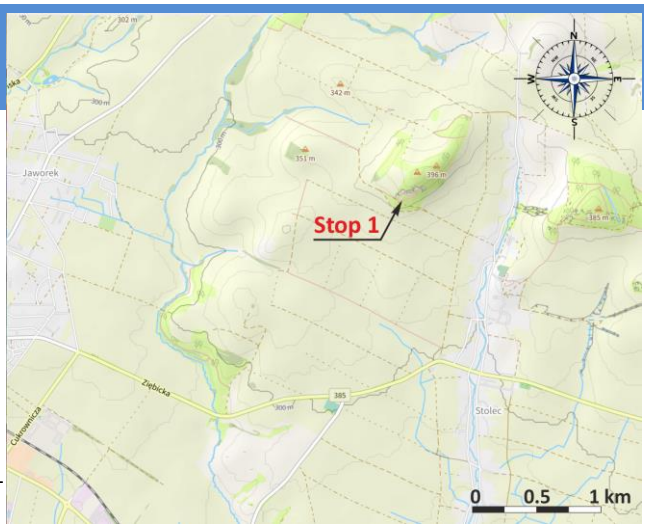

GPS coordinates: 50.5971817N, 16.8741775E

Position and lithology: volcanosedimentary succession of the Kamieniec Metamorphic Belt

Described problems: provenance,
maximum depositional age,
early Palaeozoic volcanism,
Variscan tectonometamorphic record_ _ _ _ _ _ _ _ _

Provenance and maximum depositional age

Mica schists with several centimetres to a few decimetres of felsic metavolcanites are exposed in the visited abandoned quarry in Stolec. For provenance studies, zircon age spectra of mica schists from the Kamieniec Ząbkowicki Metamorphic Belt were obtained by U-Pb LA-ICP-MS dating. The youngest detrital age population of grains indicates the maximum depositional age of these rocks at c. 529 Ma, suggesting that the sedimentary protolith of the Kamieniec Ząbkowicki metapelites were probably deposited in an Early Palaeozoic sedimentary basin (Szczepański et al., 2023; Jastrzębski et al., 2020). Zircon dating revealed a predominance of Neoproterozoic grains, representing 45 to 68% of the zircon analyses in the studied samples . The detrital zircon ages, clustered between 1.1--0.53 Ga and 2.2-1.8 Ga, with only a few Mesoproterozoic zircon ages (Fig. 5), indicate a West African and/or Trans-Saharan provenance for the studied volcanic-sedimentary rocks. (Jastrzębski et al., 2020, Szczepański et al., 2023).

Early Palaeozoic volcanism

Felsic volcanics interspersed among mica schists exposed in the KMB succession are quartzo-feldspathic, fine-grained rocks with the dominant mineral assemblage Qz + Kfs + Ms + Bt + Opq. A very fine-grained matrix (Kfs + Qz ± Ms) contains dispersed K-feldspar porphyroblasts of <2mm in diameter. In terms of chemical composition (Fig. 10a) these rocks correspond to rhyolites of subalkaline, strongly peraluminous affinity (A/CNK, A/NK: 1.1–2.3, CIPW normative corundum up to 7.6%). The rocks show enrichment in LREE ([La/Sm]CN 2.8–5.5, [La/Yb]CN = 3.8–13.6), strong Eu negative anomaly ([Eu/Eu*]CN = 0.11–0.36) but weak fractionation of MREE over HREE ([Gd/Yb]CN 1.0–1.5). Compared to the upper continental crust (Fig. 10c), they are depleted in HFSE (e.g., Nb, Zr, Ti) and in compatible elements (V, Co). The inconsistent behaviour of LILE vs. SiO_2 implies some element mobility during metamorphic events. Variations in major and trace elements suggest fractionation of plagioclase, biotite, apatite, ilmenite, and cordierite with some zircon and perhaps monazite. Alternatively, these chemical features may, at least in part, mirror the melt source, as the upper and/or middle crust displays

depletion in high-field-strength elements (Taylor and McLennan, 1985). The continental crust-related origin of metarhyolites protolith is also supported by the peraluminous, corundum-normative composition of the rocks and low Nb/Th (0.2-0.7), Zr/Nb (8-23) ratios. Moreover, a high LREE/HFSE ratio and Th concentration together with weak fractionation of MREE over HREE imply the generation of magma in a subduction-related environment. Based on petrogenetic diagrams (not shown here) we interpret that immature, quartz-feldspathic-rich sediments (greywackes or psammites originally deposited in arc environments, e.g., active continental margin) gave rise to felsic melts (Fig. 10b) which next were emplaced in a post-collisional to post-orogenic (transitional) setting. The process of anatexis was itself induced by heat input from the upwelling asthenosphere and it followed syn-collisional crustal thickening of a limited degree. Consequently, the progression of the tectonic setting from post-collisional toward anorogenic, presumably extensional regime could have taken place. The time of magmatic emplacement is estimated at late Cambrian by the dominant age 512.4 ± 4.1 Ma of metarhyolite zircons. Their rare Neoproterozoic and Archaean inherited ages (c. 560, 630 and 2588 Ma) indicate, albeit minor, involvement of an older crustal (detrital) component recycled in the magma source.

We correlate the origin of the metarhyolite protolith with other late Cambrian, S-type, peraluminous (meta-)granites from the Saxothuringian domain in the West Sudetes and those from the Moldanubian and Teplá-Barrandian domains but not the Brunovistulian domain. They mark the end of the Cadomian orogeny (arc-Gondwana continent collision) and the onset of Cambro-Ordovician rifting correlated with intrusions into transitional crust at the Gondwanan peripheries (Szczepański et al., 2023).

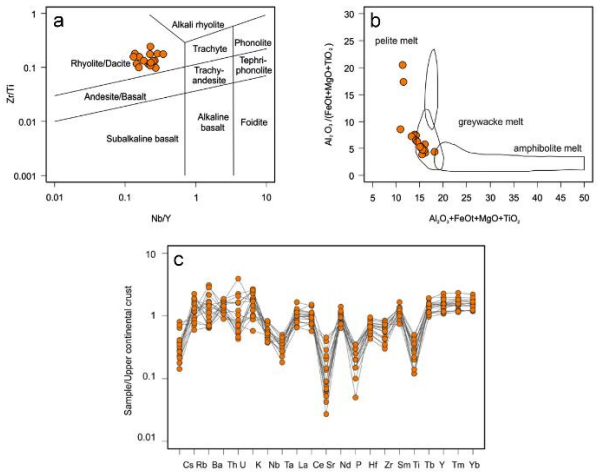

Fig. 10. Geochemical features of the meta-rhyolites of the Kamieniec Metamorphic Belt (Szczepański et al., 2023). a. Classification diagram of (Winchester and Floyd, 1977). b. diagram of (Jung et al., 2009) with fields from granitic melts generated experimentally from metapelites, greywackes and amphibolites. c. Incompatible trace elements abundances normalized to upper continental crust (Taylor and McLennan, 1985).

Variscan tectonometamorphic record

The outcrop is dominated by the S1 foliation that is deformed by the metre-scale F2 folds. Their axes are generally subhorizontal and oriented NW-SE. As a result the S1 foliation in different parts of the outcrop shows orientation varying from subvertical to subhorizontal (Fig. 11). Locally, on the steep limbs of the F2 folds the S2 subhorizontal cleavage may be observed.

The metamorphic record documented in this area was reconstructed based on sample PK007 collected c. 2 km SE of this outcrop. The mica schist sample PK007 (Fig. 12) displays millimetre-sized garnet porphyroblasts in a schistose matrix mainly consisting of quartz, K-white mica, biotite and chlorite. Accessory minerals are paragonite,

margarite, rutile, ilmenite, zircon, and apatite. In the rock matrix, millimetre-thick and strongly elongated quartz-lenses alternate with laminae composed of muscovite, rare biotite, and chlorite. However, refolded quartz lenses and white mica plates oblique to the penetrative foliation are preserved throughout the sample, giving rise to two sets of foliations (S1 and S2, Fig. 12). Similar two foliations are also occasionally preserved in garnet porhyroblasts (Fig. 8e).

Subhedral garnet porphyroblasts range from 0.2 up to 2 mm in size, and they often contain polymineralic inclusions comprising chloritoid, K-white mica and paragonite as well as margarite, clinozoisite, and quartz (Fig. 13). We interpret the latter type of polymineralic inclusions potentially as pseudomorphs after lawsonite that could have been produced according to the following mineral reaction (Chatterjee, 1976; Gomez-Pugnaire, Visona, & Franz, 1985):

$$5Lws = 2Czo + Mrg + 2Qz + 8H_2O.$$

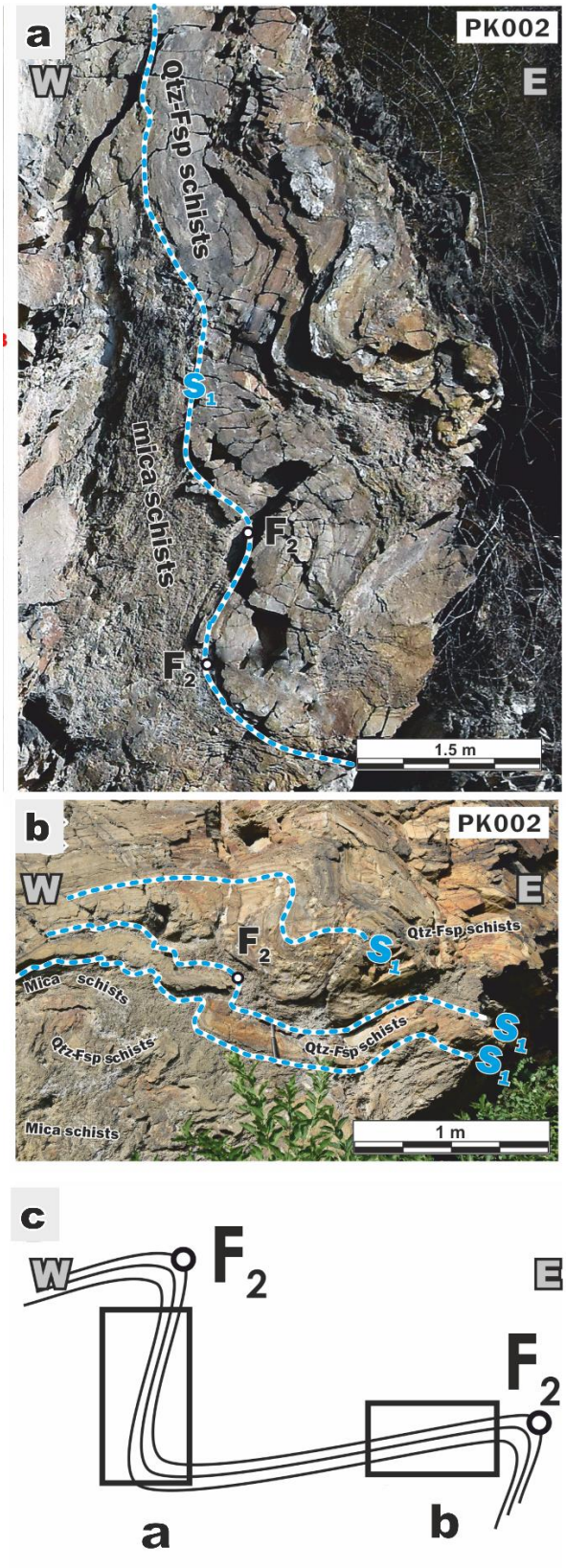

Fig. 11. (a) and (b) Field photographs documenting variably inclined older S1 fabric (blue dashed line) oriented parallel to the lithological boundaries. (c) Cartoon showing position of photographs with respect to F2 fold visible in outcrop near Stolec.

Garnet grains in the PK007 sample typically exhibit complex chemical zonation (Figs. 14), with bell-shaped spessartine profile in their core (X_{sps} decreasing from ~ 23 to 10%), sharp spessartine increase in the inner rim (X_{sps} ~ 15), followed by its decrease towards the outer rim (X_{sps} ~ 9). The variation in spessartine content is coupled with a gradual core-to-rim increase of almandine content (X_{alm} from ca. 57 to 72). Grossular concentration displays relatively low value in the inner core (X_{grs} ~ 12.5 to 17.5), which increases outwards in the most part of the outer core and rim (X_{grs} ~ 18 to 20). However, the grossular concentration decreases rapidly at the interface between outer core and inner rim, as well as in outer rim (X_{grs} ~ 14 and 10, respectively, Fig. 14 and 15). We interpret the described chemical zonation as formed in response to two distinct stages of garnet growth. We use Grt1 to denote the garnet forming the internal parts of garnet grains, and Grt2 for garnet rims. Interestingly, Grt1 entraps rutile inclusions, while Grt2 contains mostly ilmenite inclusions, indicating that both garnet types were equilibrated under different P-T conditions. This conclusion is also confirmed by the occurrence of polimineral clinozoisite, margarite and quartz inclusions within Grt1, which we have interpreted as presumed pseudomorphs after lawsonite (Fig. 13). Furthermore, chloritoid inclusions in Grt1 form blasts with grain size of up to 100 microns (Fig. 13), showing quite uniform chemical composition characterized by X(cld) [=Fe/(Mg+Fe)] ranging from 0.79 to 0.88. Additionally, rare chlorite inclusions were documented in both Grt1 and Grt2.

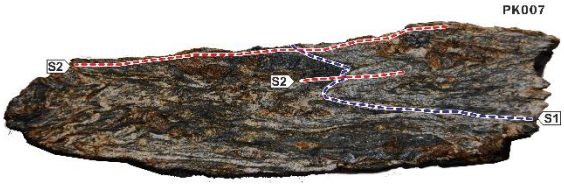

Fig. 12. Photograph showing two sets of foliations preserved in sample PK007. The older planar structure S1 is refolded.

K-white mica may be grouped into highly-abundant low Si grains for which Si content ranges from 3.0 to 3.20 apfu and a less frequent set displaying phengitic composition with Si content ranging from 3.25 to 3.45 apfu (Fig. 15). The phengitic white micas were documented in rock matrix, mostly in the microlithons, but also in the cleavage domains, and as inclusions in the core parts of garnet grains (Grt1). Low Si K-white mica grains occur abundantly in the matrix of the investigated sample, often within the cleavage domains, and they are also preserved as inclusions in the Grt2.

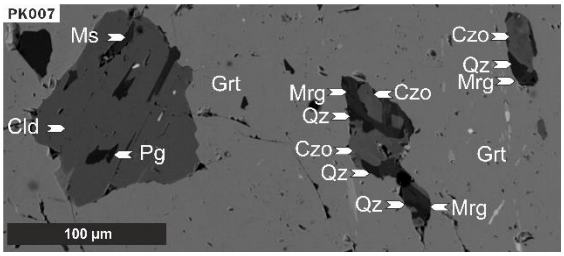

Fig. 13. Backscattered electron image showing the textures of polymineralic inclusions in garnets from sample PK007. Polymineralic inclusions consisting of Ctd + Ms + Pg and Mrg + Qz + Czo.

Plagioclase occurs in the matrix, generally forming small grains reaching up to 0.03 mm in diameter as well as porphyroblasts with diameter of up to 0.5 mm. Small matrix grains display an oligoclase composition, with maximum 22 mol% of An, and porphyroblasts show albitic cores, with developed oligoclase rims, which are well developed in the pressure shadows. Therefore, we suggest that plagioclase probably forms two generations represented by an older Pl1 with an albitic

composition and a younger Pl2 with an oligoclase composition.

Small biotite flakes were documented as inclusions in Grt2 as well matrix grains in the inspected PK007 mica schist sample. Biotite is characterized by X_{Mg} varying from 0.29 to 0.52.

Based on textural observations, we distinguish three mineral assemblages in mica schist sample PK007: the M1 assemblage represented by Grt1 and Cld + Ph + Pg + [Lws] + Chl +Rt + Qz predominantly forming inclusions in Grt1. Mineral phases reported in square brackets represent presumed pseudomorphs. Phengitic white mica, chlorite and rutile are also present in the matrix of the inspected sample. The M2 assemblage represented by Grt2 and Ms + Bt + Pl1+ Chl +Ilm + Qz is observed in the Grt2 grains as well as in the matrix and the M3 assemblage comprising Ms + Bt + Pl2+ Chl +Ilm + Qz is observed exclusively in the matrix of the inspected sample.

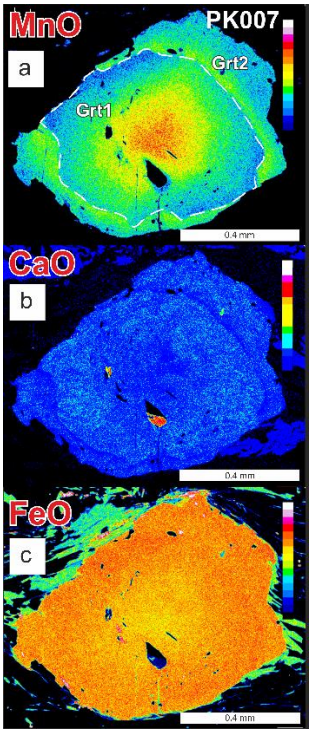

Fig. 14. X-Ray maps illustrating chemical zoning of garnet porphyroblasts from PK007 mica schist. a. Mn, b. Ca and c. Fe.

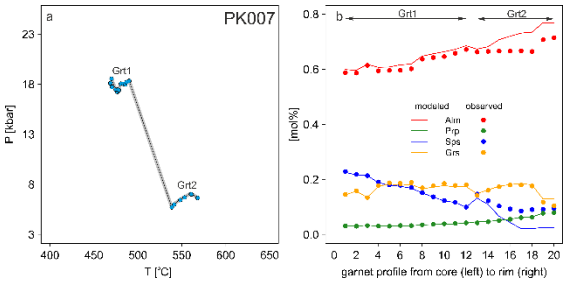

Fig. 15. Results of thermodynamic modelling for sample PK007: (a) reconstructed P-T path, (b) modeled vs measured chemical profiles in garnet. A core to rim sector of the profile was analysed.

To describe the P-T history of the PK007 sample we separately modelled the P-T history of the core (Grt1) and rim (Grt2) parts using the approach proposed by Moynihan & Pattison (2013). The obtained P-T paths and a comparison of observed and modelled garnet chemical profiles are presented in Fig. 14.

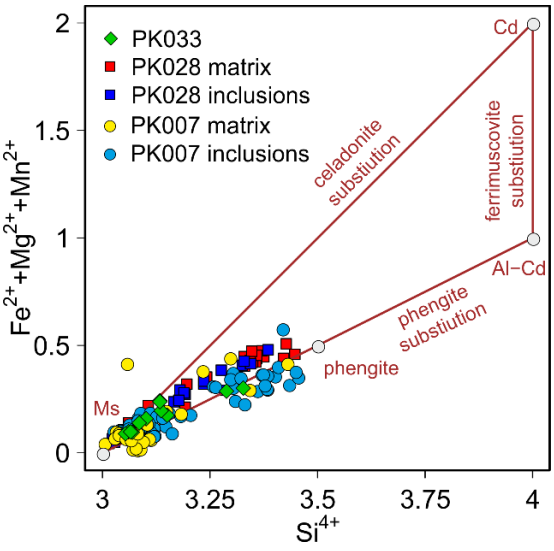

Fig. 16. Compositional variations of white micas in the investigated mica schists from the Kamieniec Metamorphic Belt.

The generally prograde P-T path for Grt1 is rather irregular. It starts at ca. 468°C and 18.1 kbar and ends at 490°C and 18.3 kbar (Fig. 15a). According to thermodynamic modelling, the core part of garnet grain (Grt1) in this sample was equilibrated within the stability field of Grt + Ph + Pg + Cld + Lws + Chl +Rt + Qz, which is consistent with the observed set

of inclusions and presumed Lws pseudomorphs preserved in garnet grains (Fig. 13).

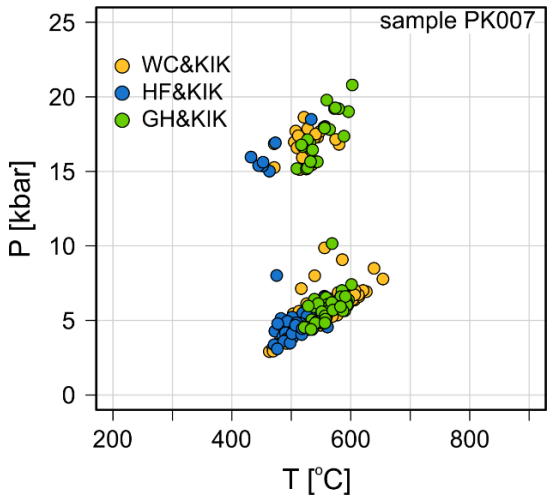

Fig. 17. Results of geothermobarometric calculations for sample PK007. KIK - Si in phengite geobarometer (Kamzolkin et al., 2016). WC - Ti in white mica geothermometer (Wu and Chen, 2015). Garnet-muscovite geothermometer in calibration of HF - Hynes & Forest (1988) and GH - Green & Hellmann (1982).

Results of thermodynamic modelling clearly indicated that during the HP stage lawsonite should be present in a relatively small amount, only slightly exceeding 2 vol%. Furthermore, X_{Mg} of chloritoid should fall in the range of 0.1 – 0.14, which agrees well with the observed composition of this mineral.

The effective bulk rock composition calculated at the end of Grt1 growth was used as an input for reconstructing of P-T conditions during Grt2 growth. The reconstructed prograde P-T path is located in low pressure region of the analysed P-T space at ca. 538-568°C and 5.7-7.1 kbar (Fig. 15a). As a result, the core of Grt2 was equilibrated in the stability field of Grt + Pl + Bt + Ms + Chl + Ilm which is compatible with commonly preserved ilmenite inclusions in Grt2, as well as plagioclase observed in the matrix of the sample. Pressure and temperature differences during the transition between Grt1 and Grt2 yields 13 kbar and ca. 50°C (Fig. 15a). According to our thermodynamic modelling, the simplest explanation for strongly limited garnet growth at the transition between Grt1 and Grt2 is that reconstructed P-T path is nearly parallel to garnet vol% isopleths. A fast decompression rate may be an additional factor suppressing garnet growth at this stage. Unfortunately, this is only a speculation as the grains of both garnet types are too small to be separately dated to test this hypothesis.

The P-T path reconstructed based on the Grt2 composition ends in the stability field of Pl2 + Grt + Bt + Ms + Chl + Ilm. However, the reconstructed PT path may constitute an incomplete record of garnet growth. A careful inspection of the chemical profiles shows a slight spessartine increase in the outer rim (Fig. 15a), and garnet grains from this sample show very irregular shapes (Fig. 14). Both observations are indicative of garnet-consuming resorption, which could be responsible for the partial dissolution of garnet grains.

According to thermodynamic modelling, the core and rim parts of garnet grains in the sample PK007 were formed in contrastingly different P-T conditions. This is confirmed by the diverse inclusion sets preserved in various parts of these garnets, including white mica. The K-white mica in sample PK007 display variable chemical composition, varying from phengite to muscovite with low Si content and paragonite (Fig. 16). To estimate the P-T conditions of white mica formation in all the analysed sample, we have applied Si in phengite geobarometer (Kamzolkin et al., 2016) coupled with Ti in white mica geothermometer (Wu and Chen, 2015). The advantage of these tools is that they are based on the composition of the same mineral. However, the Ti in white mica geothermometer was calibrated for a low-pressure mineral assemblage comprising ilmenite and sillimanite, and the latter mineral is not present in the inspected samples. Therefore, we have

supplemented these calculations by applying garnet-muscovite geothermometer in two calibrations formulated for metapelites metamorphosed at high pressures Green & Hellmann, 1982; Hynes & Forest, 1988). The results of geothermobarometric calculations are presented in Fig. 17.

The two chemical groups of white micas observed in sample PK007 occupy different textural position. The grains with the lowest Si content were mostly documented in the cleavage zones as well as in Grt2, i.e., in the rim parts of the garnet grains. Conversely, phengitic white mica grains were mostly documented in the microlithons as well as in Grt1. We suggest that the observed bimodal distribution of Si content in white micas may at least partly be a record of decompression. Given that the inferred P-T paths trend nearly perpendicular to white mica Si isopleths, the record preserved in white mica is more complete than that preserved in the chemical zoning of garnet grains.

Stop 2 – Kamieniec Ząbkowicki

GPS coordinates: 50.5276617N, 16.8795256E

Position and lithology: mica schists and eclogite of the Kamieniec Metamorphic Belt

Described problems: Variscan tectonometamorphic record

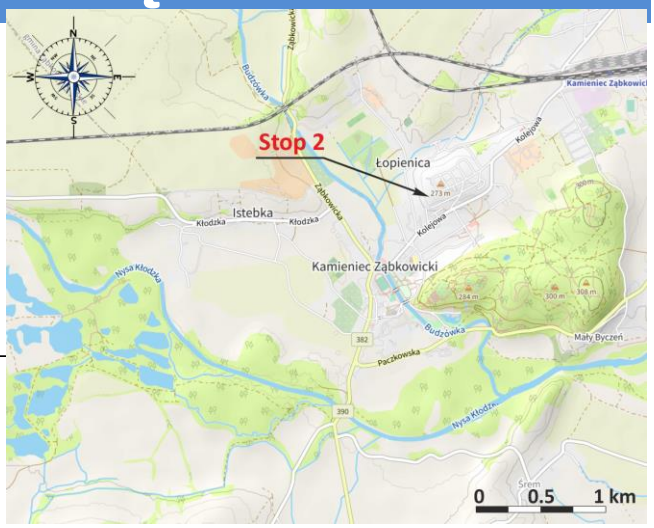

In the outcrop, small eclogite bodies (lenses, pods) are embedded in the prevailing metapelites (mica schists), however, the former ones are found in the form of loose boulders or blocks. The study of metamorphic record preserved in the outcrop was based predominantly on eclogites, nevertheless, a sample of mica schist was also collected for comparative purposes.

Petrographic outline and mineral chemical composition

Eclogites

Eclogites show random texture and are composed of garnet porphyroblasts set in the fine-grained matrix of clinopyroxene, plagioclase, amphibole, epidote, white mica and quartz. Accessory phases include rutile, ilmenite, apatite, calcite and zircon.

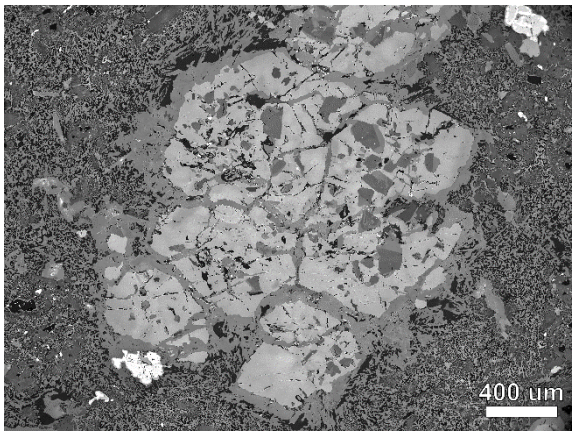

Fig. 18. Back-scattered electrons image of garnet cluster in eclogite from the KMB.

Garnet forms euhedral to subhedral porphyroblasts (up to 1.5 mm in diameter) aggregated in clusters of several crystals (Fig. 18). Porphyroblasts contain numerous, randomly distributed inclusions of clinopyroxene (omphacite), white mica (phengite), amphibole, biotite, apatite, rutile and quartz. Some of the inclusions form rectangular, poly-mineral aggregates (Ep + Am + Pg ± Qz ± Pl ± Ky; Fig. 19). We interpret them as pseudomorphs after lawsonite (cf. Orozbaev et al., 2015, Tsujimori and Ernst, 2014,

Zeng et al., 2019). Garnet shows continuous, prograde chemical zoning (Fig. 20) of spessartine (bell-shaped distribution from ca. 0.30 to 0.01 rimwards), almandine (from 0.38 up to 0.66 rimwards) and pyrope (ca. 0.01 in the core to <0.26 at the rim). Grossular does not display substantial changes in distribution across the crystals.

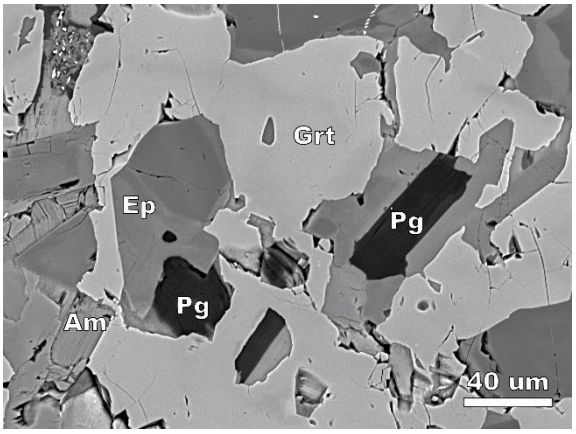

Fig. 19. Back-scattered electrons image of poly-mineral inclusions in garnet in eclogite from the KMB interpreted as pseudomorphs after lawsonite.

Matrix is dominated by omphacite variously replaced by fine-grained Cpx + Pl symplectites (Fig. 21a). The same textures are observed in the omphacite inclusions found in garnet porphyroblasts. All omphacite relics have similar composition and their XJd reaches in maximum 0.46–0.49. Clinopyroxene that replaces omphacite is less Na-rich and corresponds to diopside or augite. In turn, symplectitic clinopyroxene is partly overgrown by amphibole, which ranges from pargasite to Mg-hornblende to actinolite. This composition is in contrast to the amphiboles present as garnet inclusions or directly overgrowing garnet porphyroblasts (ferro-sadanagaite or ferro-pargasite).

White mica occurs in two types. The first one is present in the matrix or as inclusions in garnet and has the composition of phengite with Si^{4+} up to 3.49 apfu and X_{Na} <0.11 (X_{Na} = Na/(Na + K + Ca)). It is partly or completely pseudomorphed by Bt + Pl symplectites (Fig. 21b). The second type of white mica corresponds to paragonite (Si c. 3.00 apfu, X_{Na} >0.80). Its presence is confined to mineral aggregates in pseudomorphs after lawsonite.

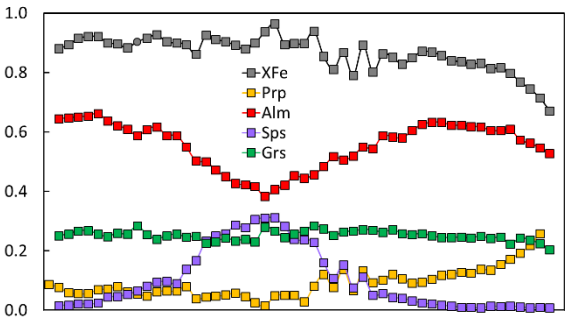

Fig. 20. Chemical variation of the representative garnet porphyroblast from the KMB eclogite.

Epidote belongs to the clinozoisite subgroup (Armbruster et al., 2006) and shows a chemical zoning with cores richer in Al than the rims. At places, crystals in the matrix have higher concentrations of REE in their cores. Plagioclase composition depends on its textural position. In Cpx + Pl symplectites it is albite, whilst in post-phengite symplectites and pseudomorphs after lawsonite the anorthite content is higher (oligoclase–andesine). Rutile forms tiny blasts in garnet and omphacite relics, however, in the matrix it occurs as elongated aggregates (up to 3 mm long). The mineral is often partly overgrown by ilmenite and titanite. Apatite was documented both as inclusions in garnet and in the matrix. Its composition is characterized by a varied concentration of F and a very low of Cl.

The textural position of the minerals and the observed breakdown structures led us to recognition of two mineral assemblages: 1) a prograde-baric peak assemblage Grt (rim) + Omp + Ph + Amp + Rt + Lws + Qz + Ap, and 2) a retrograde assemblage Cpx + Pl + Bt + Pg + Ep + Amp + Ilm-Ttn + Qz ± Ky identified in pseudomorphs after phases of the first assemblage (garnet, omphacite,

phengite, lawsonite). It appears that only garnet cores preserved the composition pertinent to the incipient stages of metamorphic progression.

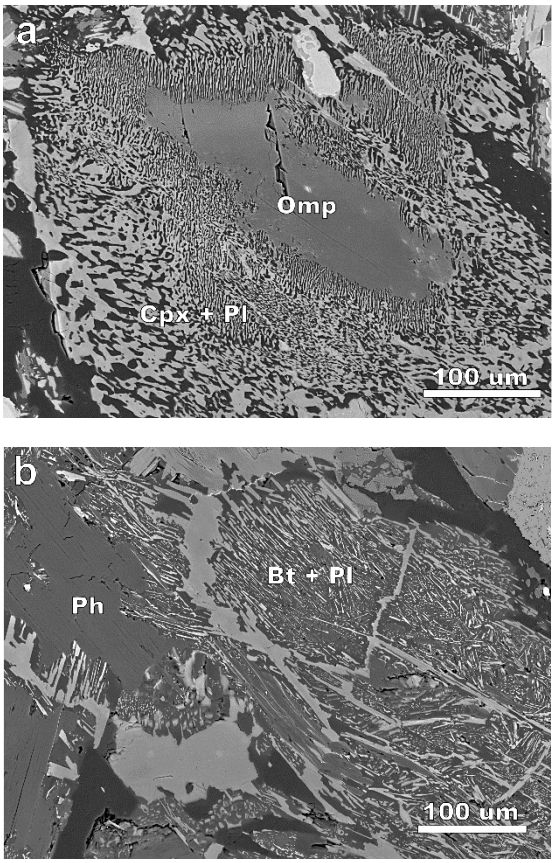

Fig. 21. Symplectites in the eclogite of the KMB: a. clinopyroxene and plagioclase after omphacite, b. biotite and plagioclase after phengites.

Mica schists

The mica schist sample comprises garnet porphyroblasts embedded in a coarse-grained, strongly laminated matrix (the S1 planes refolded by younger F2 folds) composed of quartz, K-white mica with minor biotite, andalusite, plagioclase, staurolite and chlorite. Accessory minerals are rutile, ilmenite, margarite, paragonite, chloritoid, epidote, zircon and apatite.

Subhedral porphyroblasts of garnet (4–8 mm in size) contain inclusions of chloritoid, K-white mica, paragonite, margarite, chlorite, staurolite, biotite, plagioclase, clinozoisite, rutile and quartz (Figs. 22). Parallel alignment of rutile needles marks the S1 planes in porphyroblast (Figs. 23b). Garnet blasts show prograde chemical zonation (Fig. 23a), with a bell-shaped spessartine profile (X_{sps} from ca. 0.09 in the core to nearly 0 rimwards) and a gradual core-to-rim increase of almandine (X_{alm} from ca. 0.70 to 0.80). Grossular concentration is stable in the inner core (X_{grs} 0.18–0.21) but decreases sharply outward (X_{grs} 0.08–0.10). Pyrope content gradually increases rimwards (X_{prp} from ca. 0.04 to 0.14).

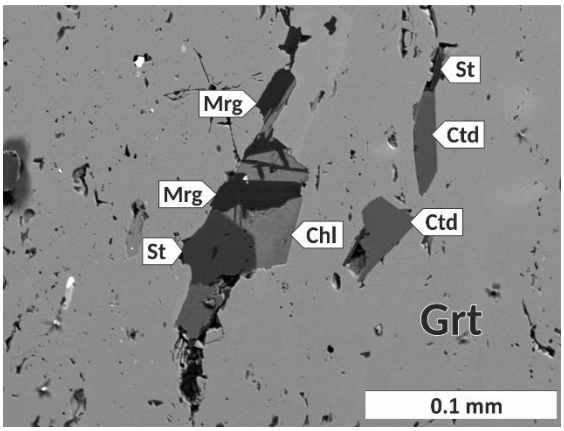

Fig. 22. Back-scattered electrons image of poly-mineral inclusions in garnet in mica schist from the KMB.

Two types of K-white mica are present: 1) blasts with high Si content (up to 3.44 apfu) which are aligned parallel to the S1 foliation, 2) blasts with low Si content (ca. 3.10 apfu; Fig. 24) mostly documented within the axial planes of the F2 folds.

Plagioclase grains in the matrix have albite composition, while the inclusions in garnet are richer in anorthite content (oligoclase). Biotite and rare chlorite blasts present in the rock matrix are richer in Mg than their inclusions in garnet. Staurolite found in the matrix shows homogeneous chemical composition (X_{Mg} = 0.13–0.17), but inclusions in garnet are varied compositionally (X_{Mg} = 0.04–0.15).

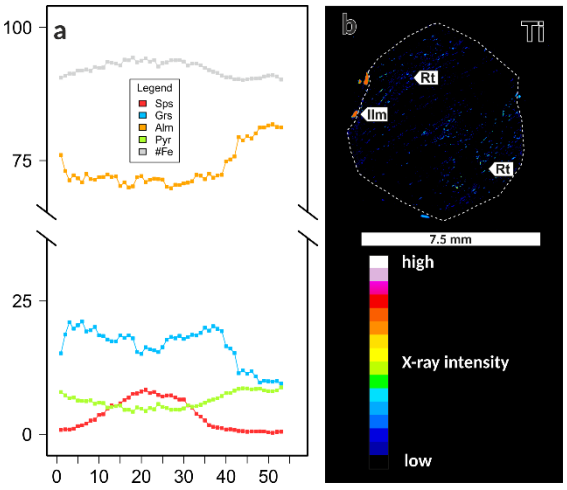

Fig. 23. a. Chemical variation of the representative garnet porphyroblast from the KMB mica schist. b. X-Ray map of Ti illustrating rectilinear inclusion trails of rutile preserved in garnet porphyroblast from PK023 mica schist

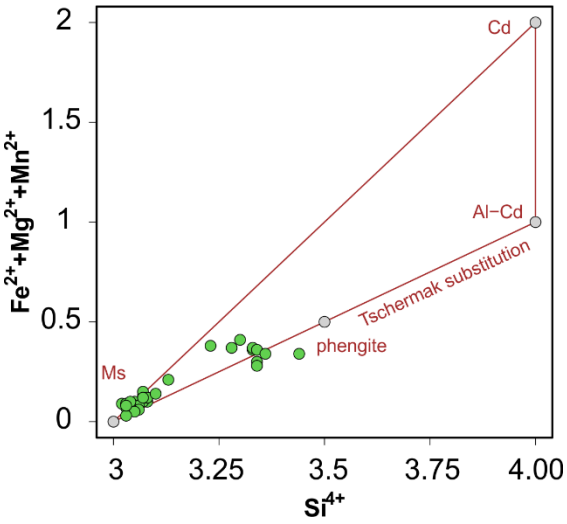

Fig. 24. Compositional variations of white micas in the investigated mica schists from the Kamieniec Metamorphic Belt.

Finally, we distinguish two mineral assemblages in the investigated mica schist: 1) M1 assemblage mostly occurring as inclusions in garnet porphyroblasts (Grt + Cld + Ph + Pg + Chl +Rt + Qz), 2) M2 assemblage observed as inclusions in garnet and in the matrix (Ms + Bt + Mrg + Pl + St + Ilm + And + Qz).

Metamorphic record

Eclogites

The P-T path reconstructed for eclogites is shown in Fig. 24. The prograde segment up to baric peak is based on thermodynamic modelling of phase equilibria, while the second part of the loop is derived from conventional geothermobarometry. The first stage was estimated by intersection of isopleths for relic Mn-rich core of garnet and yielded 470°C and 12–13 kbar. The following stage of metamorphism was reconstructed with reference to the composition of Grt (rim) + Ph + Omp and taking into account the chemical fractionation of the rock by the progressive growth of garnet. The compositional isopleths for the minerals of the metamorphic peak assemblage indicate pressure from 24 to 27 kbar in a narrow temperature range of 550–570°C. The model shows that lawsonite joined the mineral assemblage during the prograde portion of the P-T loop. It also predicts that the abundance of lawsonite was <5 vol.% at the baric peak conditions. Thus the lawsonite-out boundary sets the low-P limit of the inferred P-T conditions with the implication that lawsonite must have disappeared with the onset of retrogression. These inferences are compatible with our textural observations and interpretation of poly-mineral inclusions in garnet (Fig. 24).

The estimation of HP conditions by means of conventional geothermobarometry confirmed these results. A selection of calibrations for Grt + Cpx (Omp) in quartz-bearing and kyanite-free mineral assemblage yielded pressures of ca. 24 kbar at ca. 550°C. We also used Raman elastic barometer for apatite inclusions in garnet (AiG) aiming at independent estimation of pressure conditions. The calculated composition-corrected entrapment

pressures of apatite inclusions combined with the Zr-in-Rt geothermometer (Kohn, 2020) for rutile inclusions point to pressures of ca. 23 kbar and validate the above results.

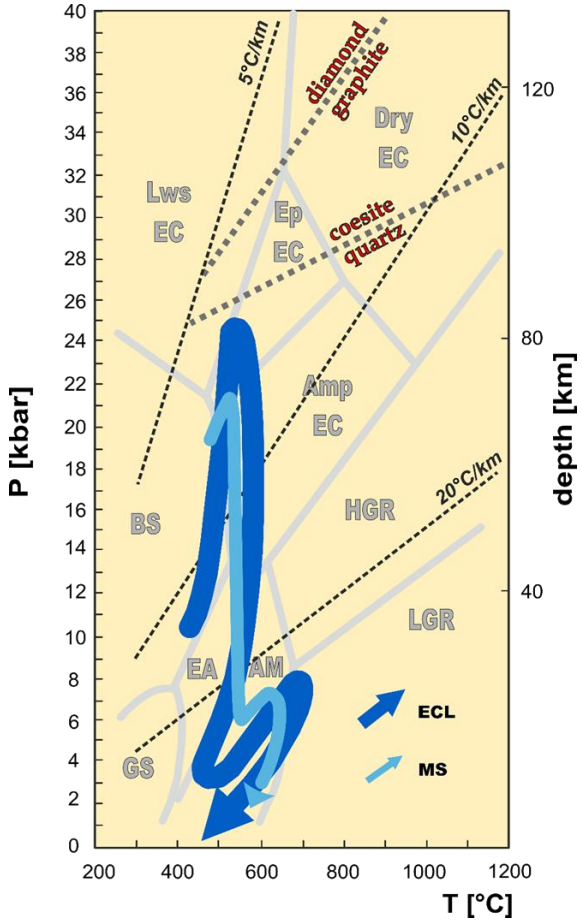

Fig. 24. The P–T path reconstructed for the studied eclogites (ECL) and the sample of the mica schists (MS) from the KMB.

The subsequent stages of metamorphism seen in the outcrop are predominantly documented by compositional changes in amphibole ± plagioclase. They show second progression of metamorphic conditions starting at <3.5 kbar and <550°C up to-medium pressures (ca.7 kbar) reaching a thermal peak of 650-690°C. The final exhumation stage must have ended the P–T trajectory at shallow crustal levels.

Mica schists

The reconstruction of P-T path for the mica schist sample was based on garnet composition (Fig. 24). The calculation show that growth of garnet started at c. 480°C and 19.5 kbar and continued up to c. 520°C and c. 21 kbar. The model predicts the Si content in white mica of ca. 3.40 apfu, which corresponds directly with our mineral-chemical observations. The calculations suggest that lawsonite (<2 vol.%) was present at the onset of garnet crystallization but subsequently it reacted out. This is consistent with the lack of lawsonite in the mica schist studied.

Moreover, calculations imply that phases post-dating garnet growth (Pl + low-Si Ms + St + Ilm) are related to a pressure drop to ca. 5–8 kbar (Fig. 24). The composition of the model-predicted white mica (Si ca. 3.05 apfu) and staurolite (X_{Mg}: 0.12–0.14) is in good agreement with the respective minerals present in the matrix. The topology of the staurolite model isopleths suggests a P–T increase from ca. 530°C and 6 kbar to ca. 640°C and 6–7 kbar. In turn, the presence of andalusite points to a subsequent drop in pressure to <4 kbar at ca. 600°C.

The contrastingly different P-T conditions experienced by the mica schist sample during metamorphic evolution suggested by thermodynamic modelling, were consistently confirmed by conventional geothermobarometry based on white mica and garnet mineral composition. The applied combination of calibrations of geothermobarometers devised for Grt + Ph + Ms metapelites indicate that phengitic white micas crystallized predominantly at ca. 13-20 kbar, while the low-Si white mica flakes equilibrated at pressures of c. 3-10 kbar (Fig. 24).

Summary

Nearly identical metamorphic evolution and the shape of P–T path were obtained for eclogites and mica schists collected from the same outcrop. The metamorphic evolution was multistage and defines

a clockwise P–T trajectory that comprises a prograde segment up to the baric peak (HP-LT episode, cold subduction), then a retrogression path followed by a LP-HT episode (thermal peak) and terminates with a final exhumation to shallow crustal levels.

Stop 3 – Doboszowice

GPS coordinates: 50.5002281N, 16.9589100E

Position and lithology: orthogneiss of the Doboszowice Metamorphic Complex

Described problems: early Palaeozoic magmatism,

Variscan metamorphic record

Early Palaeozoic magmatism

In the abandoned quarry at Pomianów Górny the Doboszowice orthogneiss is exposed. It is two-mica, medium-grained L-tectonite, composed of quartz, plagioclase, K-feldspar, muscovite, biotite and accessory garnet. The magmatic protolith of the Doboszowice orthogneiss was formed during the Cambro-Ordovician tectono-magmatic event, similar to other orthogneisses of the West and Central Sudetic part of the Bohemian Massif. The published isotopic zircon data from the Doboszowice orthogneisses show U-Pb ages of 488 ± 6 Ma (Concordia age, U-Pb SHRIMP, Mazur et al., 2010), 494 ± 5 Ma (Concordia age, U-Pb LA-ICPMS, Jastrzębski et al., 2023) and 500 ± 16 Ma (upper intercept age, U-Pb LA-ICPMS, Jastrzębski et al., 2023) (Fig. 25). Inherited age populations are very abundant and cluster at c. 540 Ma, 560–550 Ma, 605–585 Ma (most prominent), and 1.9 Ga (Jastrzębski et al., 2023), which generally concurs with the main features of detrital zircon age spectra of Early Paleozoic metasedimentary rocks visited during this excursion. The Doboszowice orthogneiss contains inserts of metasedimentary rocks of unknown protolith age (Jastrzębski et al., 2023, Fig. 25a). These orthogneisses are geochemically Si-rich (73-78 wt% of SiO_2), calc-alkaline and peraluminous with A/CNK ranging from 1.05 to 1.35, which suggest that they originated from melting of a sedimentary rock (Buriánková et al., 1999). At the geotectonic discrimination diagrams, the Doboszowice orthogneisses occupy a field of volcanic arc granite, close to the boundaries with ocean-ridge granites and within-plate granites (Mazur et al., 2010). Oxygen isotopic composition in c. 500-495 Ma old zircons indicate δ18O values that are generally higher than those of the primitive mantle (Fig. 25b and c), which confirms a Si-rich composition of the parent magma. This observation and abundance of the inherited zircons imply a predominant contribution from a Neoproterozoic continental crust in magma formation.

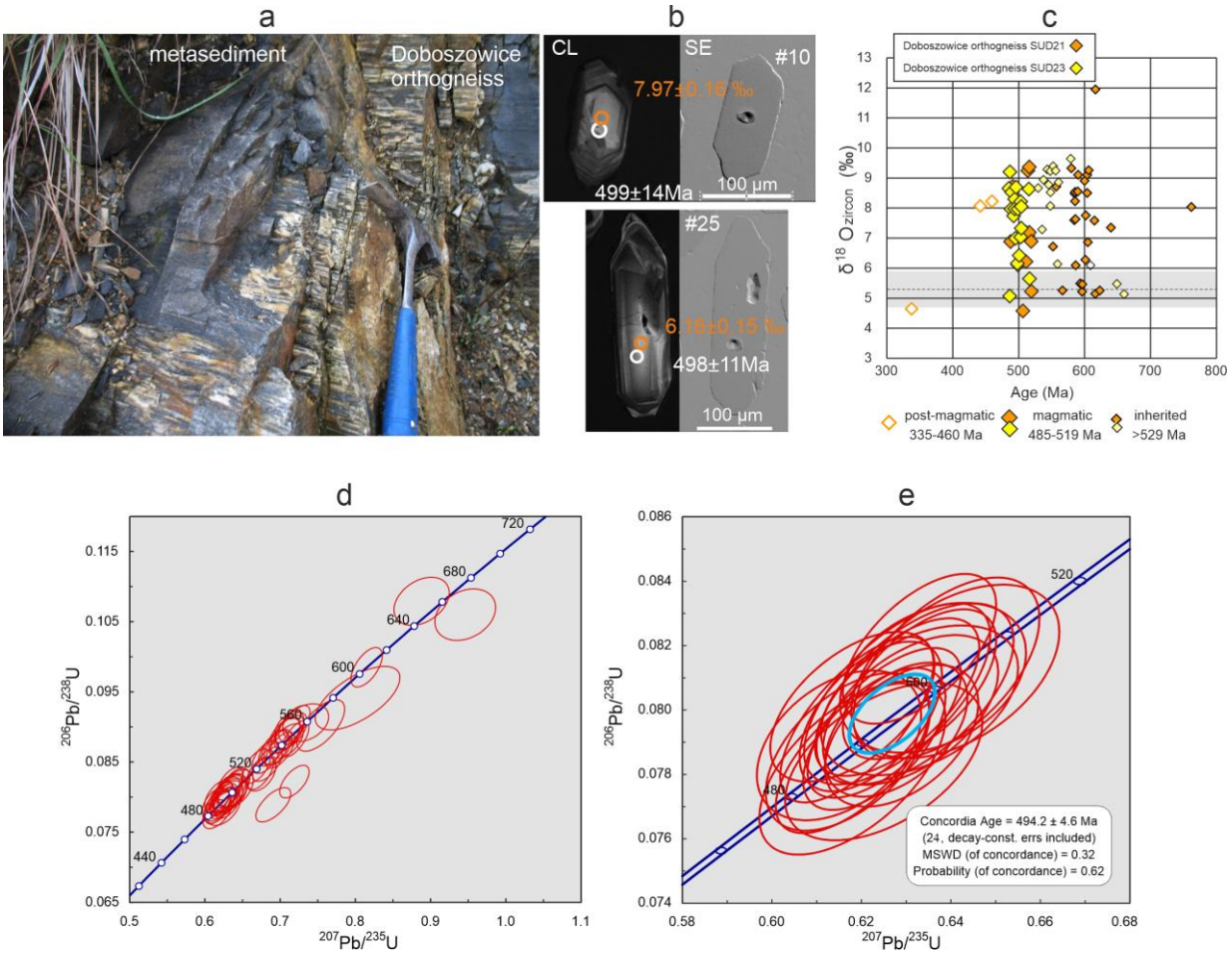

Fig 25. a) The Doboszowice orthogneisses contacting with metasedimentary rocks (Doboszowice quarry). b) U-Pb and O isotopic data in representative 500 Ma zircon grains. Spot labels of U-Pb dates (white) and O isotope data (orange). c) Results of δ18O isotopic analysis in zircon. Mantle-equilibrated value for δ18O in zircon (5.3 ± 0.6‰, 2σ, Valley, 2003) is indicated by grey color. d). Concordia U-Pb plot for the sample SUD23 collected in the visited quarry. e) Concordia U-Pb plot in the early Palaeozoic range for the same sample.

Variscan metamorphic record

The outcrop is composed of the orthogneiss consisting of quartz, K-feldspar, plagioclase, white and dark micas, and rare garnet grains. Accessory minerals are zircon, apatite and ilmenite.

The rock consists of partly recrystallized K-feldspar porphyroclasts (up to 1.5 cm in size, X_{Or} 94–99) and quartz laminae (0.5–1 mm thick) alternating with lenses composed of completely recrystallized plagioclase and thin biotite–muscovite layers. Plagioclase shows relatively stable composition (X_{Ab} 0.88–0.91). Small garnet grains (0.1–0.3 mm in size) display generally flat core chemical profile and are rich in almandine (Fig. 26, X_{slm} 63–70, X_{prp} 1–3, X_{grs} 18–30, X_{sps} 2–10; Table).

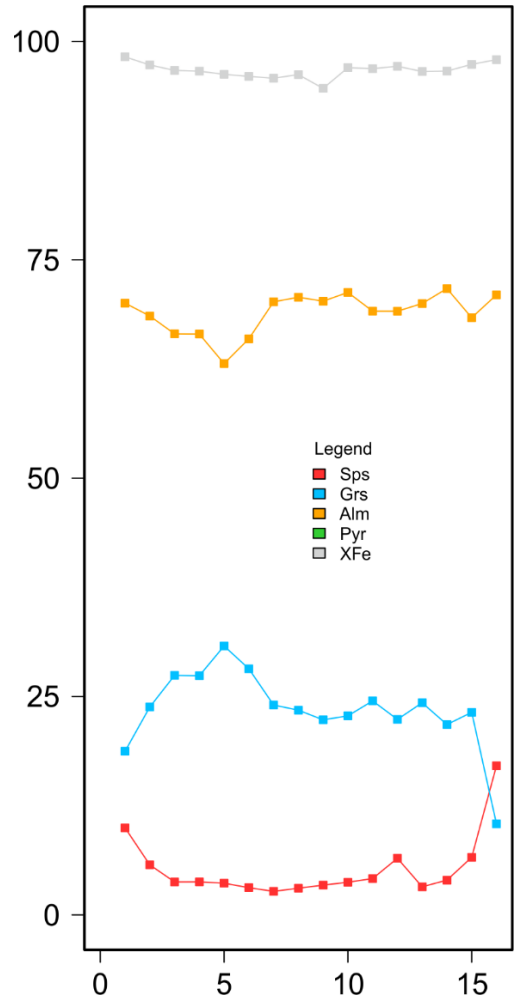

Fig. 26. Chemical zoning of representative garnet grain from sample MD09-02.

On the other hand, compared to the core, the chemical composition of the rim is characterised by a marked increase in spessartine, coupled with a decrease in grossular content and variations in almandine content. In terms of chemical composition white mica can be divided into two groups differing by Si content (Fig. 27). Abundant group Ms1 displays phengitic composition and is characterized by Si content ranging from 3.22 to 3.37 apfu and usually forms core parts of white mica grains (Fig. 27). The group Ms2 shows considerably lower Si content falling in the range of 3.11 to 3.15 apfu and forms mostly rim parts of white mica flakes. Biotite has X_{Mg} = 12–20% and Ti = 0.05–0.29 apfu. Apatite is a common accessory mineral, while ilmenite occurs extremely rare.

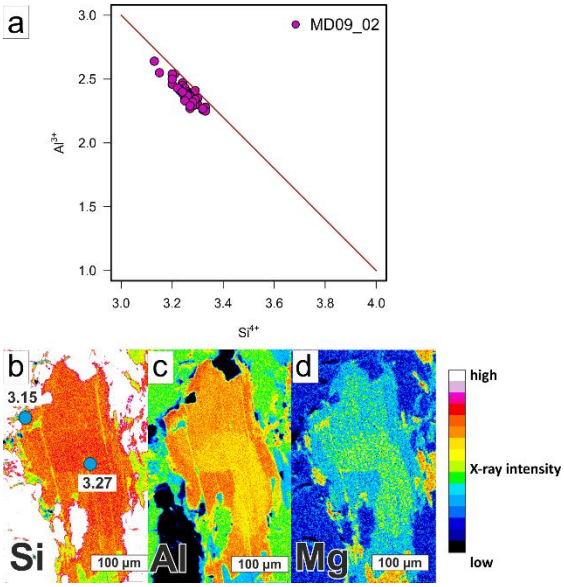

Fig. 27. X-Ray maps illustrating chemical zoning of white mica from sample MD09-02. a. Si, b. Al and c. Mg.

Based on textural observations we distinguish two mineral assemblages in the MD09-02 orthogneiss sample. The M1 assemblage is represented by white mica Ms1, with relatively high Si content corresponding to a possible high–P history of the rock. The M2 assemblage comprises Grt + Ms2 + Bt + Pl+ Kfs + Ilm + Qz.

Orthogneiss sample MD09-02 contains small garnet grains with strongly diffusionally modified profiles, which prevent calculation of a P–T path based on garnet composition. However, the calculated pseudosection coupled with isopleths corresponding to the composition of the garnet core allows estimation of maximum temperature and pressure of diffusional equilibration of garnet (Fig. 28a).

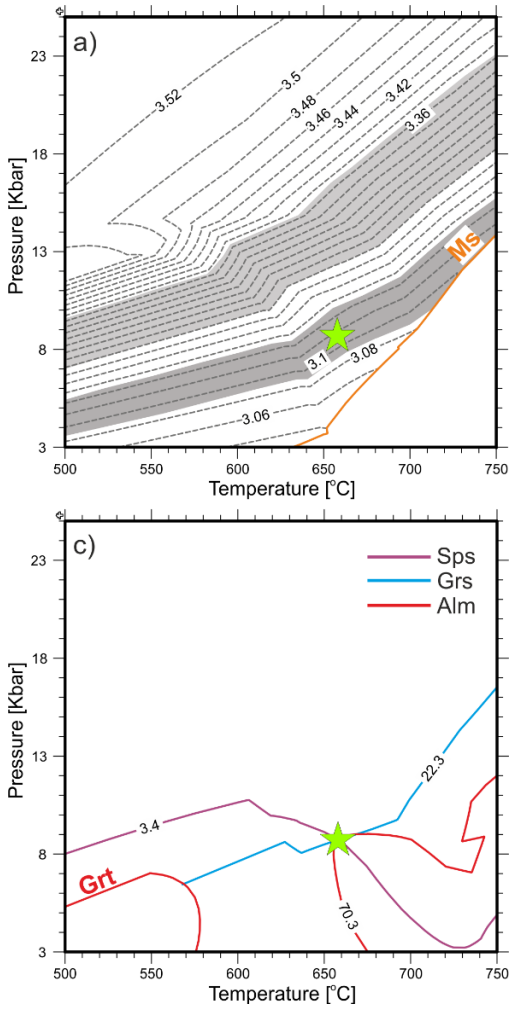

Fig. 28. Phase diagram modelling results for sample MD09-02 using the core composition of Grt and bulk rock composition; a. compositional isopleths of Si in K- white mica. Ms-out reaction is additionally shown. The composition of observed white mica flakes is indicated by grey areas. b Isopleths shown for almandine (red), grossular (blue), and spessartine (purple). Green star at the intersection of isopleths marks P–T conditions of garnet requilibration during HT metamorphism at the thermal peak of the M2 metamorphism. Green star is also shown on diagrams a and b.

Isopleths calculated for the garnet core indicate that it was stable at c. 9 kbar and 660°C (Fig. 28b).

The results of the conventional geothermobarometry show that the two compositional K-white mica groups i.e. with high and low Si content identified in the orthogneiss sample equilibrated at contrastingly different PT conditions (Fig. 29). White mica Ms1 with high Si contents shows pressures of its formation in the range of c. 16 to 22 kbar at ~590 to 720°C. On the other hand, low Si white mica Ms2 is characterized by pressures of its formation ranging from ~6 to 11 kbar at ~500 to 700°C. Consequently, textural relationship between the two compositional white mica groups support our suggestion that the observed distribution of Si content in white micas may represent a record of the MP–HT event overprinting the earlier HP metamorphic episode. The only important discrepancy that becomes apparent when comparing the results of white mica geothermobarometry with thermodynamic calculations is that the P–T conditions for white mica Ms1 from orthogneiss generally indicate high temperatures of its formation. This is the function of high Ti contents of the inspected white mica grains. However, it appears that temperature calculations for white mica Ms1 should be taken with caution, as the M1 mineral assemblage lacks ilmenite and Al_2SiO_5 phase, which are prerequisite for the application of this tool.

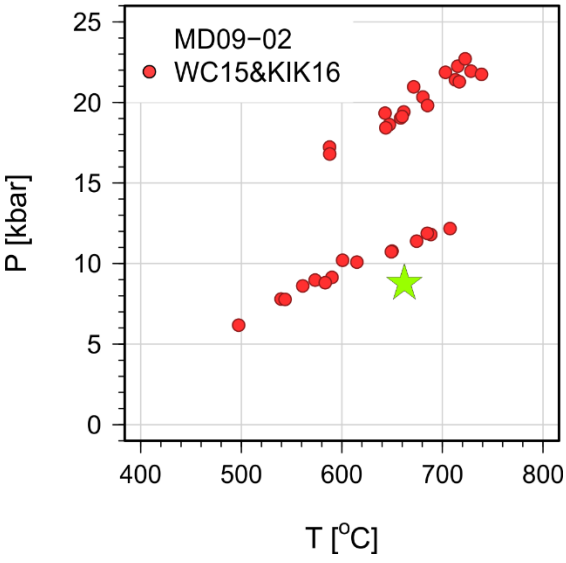

Fig. 29. Results of geothermobarometric calculations for sample MD09-02. KIK16 – Si in phengite geobarometer (Kamzolkin et al., 2016). WC15 - Ti in white mica geothermometer (Wu & Chen, 2015).

Stop 4 – Chałupki

GPS coordinates: 50.4864144N, 17.0045381E
Position and lithology: paragneiss
of the Doboszowice Metamorphic Complex
Described problems: provenance,
maximum depositional age,
Variscan tectonometamorphic record

Provenance and maximum depositional age

The Chałupki paragneisses are migmatitic, medium- to coarse-grained foliated rocks, composed of quartz, plagioclase, muscovite, biotite and garnet. In the visited part of the abandoned quarry, the paragneisses are intercalated with garnitiferous mica schists.

Detailed petrography of both rock types is described in the section devoted to Variscan tectonometamorphic record. The LA-ICP-MS zircon dating for the Chałupki paragneiss showed predominance of Neoproterozoic zircons, similar to the mica schists exposed in the Kamieniec Metamorphic Belt (Jastrzębski et al., 2023, Szczepański et al., 2023) (Fig. 5). The source area(s) for the sedimentary basin consisted of Cryogenian to Ediacaran crystalline rocks, with some Palaeoproterozoic component, but lacking Mesoproterozoic zircons. The provenance studies on the migmatitic Chałupki paragneiss thus indicate that the deposition of their sedimentary protolith took place in the western and/or northern African periphery of Gondwana (Jastrzębski et al., 2023, Szczepański et al., 2023). However, in contrast to the Kamieniec Ząbkowicki mica schists, the Chałupki paragneisses contain an additional Early Ordovician age cluster which makes up c. 10% of the zircon population. This, 510–488 Ma age cluster is formed by the most euhehral zircon crystals that might either come from erosion of the adjacent Cambro-Ordovician orthogneisses (Szczepański et al., 2023) or represent synsedimentary volcanogenic/pyroclastic admixture accompanying the sediment deposition (Jastrzębski et al., 2023). According to these interpretations, the youngest zircon age peak in the Chałupki paragneisses represents either the maximum depositional age, or the depositional age.

Variscan tectonometamorphic record

The outcrop is dominated by generally subhorizontal the S1 foliation that is locally deformed by centimetre-scale the F2 folds. Their axes are generally subhorizontal and oriented NNW-SSE. On the S1 foliation there are preserved two mineral lineations. The L1 lineation is marked by parallel alignment of white mica flakes, while the S2 lineation is marked by elongated feldspar patches.

Two samples – the mica schist MD01-18 and the paragneiss MD01-02 were investigated to decipher P-T history of the volcano-sedimentary succession exposed in the eastern part of the DCM.

Petrography and mineral chemistry of the mica schists from the Doboszowice Metamorphic Complex

The mica schist sample MD01-18 contains garnet porphyroblasts in a schistose matrix comprising quartz, K-white mica, biotite, margarite, staurolite and kyanite. Accessory minerals are rutile, ilmenite, zircon, apatite and tourmaline.

Subhedral garnet porphyroblasts range from 1 to 9 mm in size and they often contain inclusions of quartz, K-white mica, staurolite, tourmaline, ilmenite, and sporadically rutile. Garnet grains in the MD01-18 sample typically exhibit prograde growth chemical zonation (Fig. 30a),

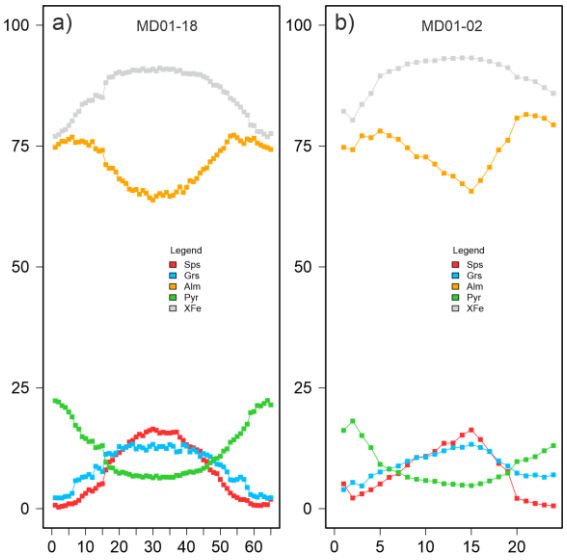

Fig. 30. Chemical zoning of representative garnet grains from: a) mica schist sample MD01-18 and b) paragneiss sample MD01-02. XFe = Fe/(Fe + Mg).

with bell-shaped spessartine profile (X_{sps} decreasing from ~ 16 to nearly 0) coupled with a gradual core-to-rim increase of almandine (X_{alm} increasing from ~ 66 to 76) and pyrope (X_{prp} increasing from ~ 6 to 22) content. Grossular concentration displays relatively stable value in the core (X_{grs} ~ 11 to 13), and decreases outwards (X_{grs} ~ 2). A small increase in X_{sps} content associated with decrease of X_{alm} and X_{prp} is observed in the outermost rim, which is characteristic of a resorption process operating during late metamorphism (e.g. Anderson and Buckley 1973). In terms of Ti-bearing phases garnet grains in this sample entrap mostly ilmenite inclusions with preserved relics of rutile in their cores (Fig. 31a). However, sporadically rutile needles are observed in the rim parts of garnet grains (Fig. 31b). Furthermore, larger ilmenite grains present in the rock matrix also contain rutile inclusions.

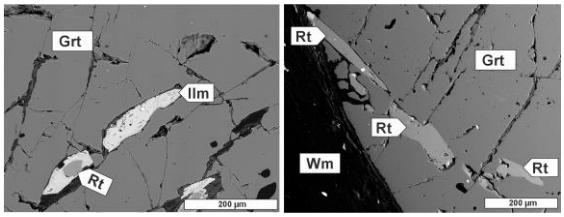

Fig. 31. Backscattered electron images of Ti-bearing phases preserved (a) as inclusions of ilmenite overgrowing rutile in a garnet from the sample MD01-18 and (b) as rutile inclusions in the resorbed rim portion of a garnet from sample MD010-18.

White mica may be grouped into four chemical varieties represented by: (i) scarcely preserved K-white mica flakes Ms1, that were documented both in the core parts of larger K-white mica plates or as isolated grains mostly preserved within quartz layers, with Si content falling in the range between 3.18 and 3.38 Si apfu (Figs. 32a and d), (ii) highly-abundant, reaching up to 3 mm in length, K-white mica grains Ms2 with Si content ranging from 3.08 to 3.15 apfu forming rims of Ms1 grains or isolated larger flakes (Figs. 32a, b and d), (iii) fine-grained

aggregates of K-white mica flakes Ms3 with Si content ranging from 3.0 to 3.05 apfu forming isolated clusters and rims developed around Ms2 white mica flakes, staurolite or kyanite (Figs. 32b, c and d) and (iiii) margarite grains Mrg with X_{Mrg} ranging from 65 to 90 ml% forming fine-grained aggregates surrounding kyanite crystals and often associated with Ms3 white mica (Fig. 32c and d). Documented margarite aggregate is characterized by paragonite content reaching up to 19 mol%. Ti content varies from 0 (for Mrg) to 0.06 for the K-white micas Ms1 to Ms3.

Plagioclase occurs sporadically forming small grains reaching up to 0.03 mm in diameter or larger porphyroblasts up to 1 mm in diameter. Documented grains reveal a diverse chemical composition and are represented by: (i) oligoclase ranging from 9.5 to 11.2 mol% of X_{An} and (ii) albite with maximum 1.7 mol% of X_{An}. Small staurolite crystals, up to 0.2 mm in size, occur as inclusions in white mica Ms2 and as inclusions in garnet grains. It is characterized by XMg between 6 and 19. Kyanite blasts range from 0.25 mm to 0.5 mm and occur mostly as inclusions within K-white mica Ms2. Some kyanite blasts are surrounded by fine-grained aggregate composed of margarite and K-white mica Ms3 (Fig. 32c). Small biotite flakes documented in the rock matrix are characterized by XMg varying from 31 to 43.

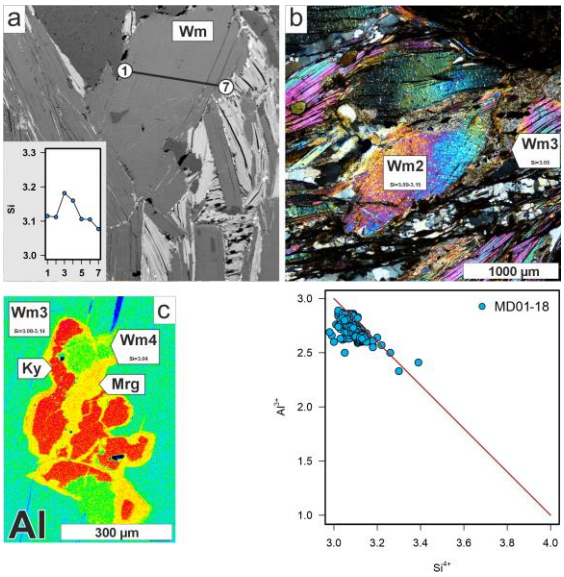

Fig. 32. (a) Backscattered electron image showing white mica Ms1 overgrown by white mica Ms2. Inset shows Si content along profile 1-7. (b) large white mica Ms2 overgrown by fine-grained white mica Ms3. (c) X - Ray map of Al distribution showing kyanite replaced by mixture of margarite (Mrg) and low-Si K white mica (Wm3) from sample MD01-18. (d) Compositional variation of white micas in the MD01-18 mica schist sample from the DMC.

Based on textural observations, we distinguish three mineral assemblages in the mica schist sample MD01-18. The M1 assemblage is represented by relics of phengitic white mica Ms1 scarcely preserved in the matrix and rutile that is preserved within core parts of larger ilmenite grains. This mineral assemblage may be indicative of relatively high–P history of the inspected sample. The M2 assemblage is represented by Grt and Ms2 + Pl + St + Ky + Bt + Ilm + Rt. The M3 mineral assemblage is represented by Ms3 + Mrg.

Petrography and mineral chemistry of the Chałupki paragneiss

The sample MD01-02 is a coarse-grained, garnet-bearing paragneiss composed of garnet, quartz, plagioclase, white mica, biotite, chlorite, and accessory ilmenite, rutile, apatite, xenotime and

zircon. Garnet grains are anhedral and reach a maximum of 4 mm in diameter. They display clear chemical zonation with bell-shaped spessartine profile (X_{sps} decreasing from ~ 16 to 2) coupled with a gradual core-to-rim increase of almandine (X_{alm} increasing from ~ 66 to 78) and pyrope (X_{prp} increasing from ~ 4 to 18) content. Grossular is gradually decreasing from core to rim (X_{grs} ~ 13 to 4) (Fig. 30b). Occasionally, there is observed a small increase in X_{sps} associated with X_{prp} and X_{alm} decrease in the outermost rim, suggesting that chemical composition of some garnet rims were locally modified by resorption (Fig. 30b, e.g. Anderson and Buckley 1973). Garnet grains in this sample contain mostly ilmenite inclusions. However, sporadically rutile needles are observed in the resorbed rim parts of garnet grains or within late cracks. Interestingly, Ti-bearing phases form mostly separate grains. However, in places where rutile and ilmenite are in contact their textural relationships may indicate simultaneous growth.

White mica flakes are 0.5–3.0 mm long and are characterized by variable Si content. Those flakes with Si varying from 3.15 to 3.22 apfu correspond to white micas Ms1 (forming core parts of the analysed plates). Those flakes with Si content below 3.15 apfu (forming rims of the analysed plates) correspond to Ms2 K-white mica observed in the MD01-18 sample (Fig. 33). Rare biotite grains are 0.3 mm long and display XMg in the range of 32–47, and Ti ranging from 0.01–0.14. Plagioclase occurs exclusively in the matrix as blasts reaching up to 3 mm, and its composition varies from albite to oligoclase (X_{An} 7 to 16). Chlorite mostly fills late cracks within garnet grains and sporadically occurs as isolated grains in the rock matrix.

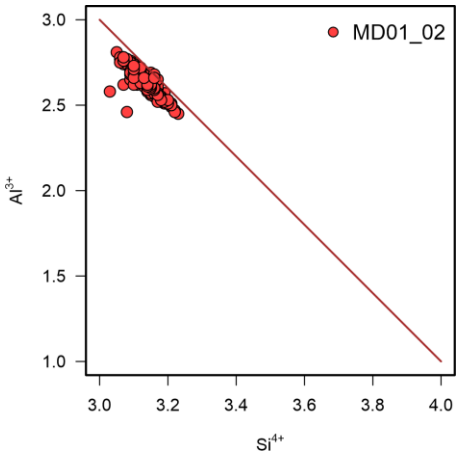

Fig. 33. Compositional variation of white mica in the MD01-02 paragneiss sample from the DMC.

Based on textural observations, we distinguish two mineral assemblages in the paragneiss sample MD01-02 that are represented by the M1 assemblage comprising rare Ms1 grains and the M2 assemblage composed of Grt and Ms2 + Pl + Bt + Rt + Ilm.

P-T history of the Chałupki paragneiss and the mica schist inlier

Sample MD01-18

The reconstructed P–T path for garnet from sample MD01-18 is shown in Fig. 34. Our calculations indicate that garnet growth started at 525°C and 4.0 kbar and ceased at 660°C and 8.0 kbar within the stability field of garnet, plagioclase, K-white mica, biotite, kyanite and ilmenite, at the lower stability limit of the melt and very close to the lower stability limit of rutile (Fig. 34). Furthermore, the reconstructed P–T path intersects the staurolite stability field. The described set of mineral stability fields intersected by the reconstructed P–T path is generally consistent with the M2 mineral assemblage documented in the inspected sample. The only lacking mineral included in the M2

assemblage is rutile. However, it is preserved in the resorbed rim portion of garnet grains or in the rock matrix. Consequently, the presence of rutile clearly indicates that both P and T must have slightly increased (c. 0.5 kbar and 10-20°C) after garnet growth ceased. This appears to be consistent with the modelled final step of garnet growth, which shows a slight increase in P and T (Fig. 32).

Furthermore, the inspected mica schist also contains a few white mica plates with relatively high Si contents, ranging from 3.18 to 3.38 apfu (Fig. 30), implying pressures of metamorphism of c. 12 to 25 kbar in the analysed temperature range of 500–750°C based on compositional isopleths (Fig. 32). Provided that phengitic white micas mostly form core parts of Ms2 white mica plates, they appear to be a record of a P–T history preceding garnet growth. This history was most likely characterised by temperatures at least below c. 640°C as the inspected mica schist show no evidence of melt formation. Otherwise, according to thermodynamic calculations, a large part of the metamorphic history of the investigated sample would have taken place in the melt stability field. Consequently, the maximum pressures of the M1 event would be between 12 to 25 kbar in the temperature range of 500 to max. 640°C.

The inspected sample also contains margarite, which was most likely formed on the retrograde path after garnet formation. Considering the textural position of margarite, it was most probably formed as a partial pseudomorph after kyanite as a result of external CaO supply following the simplified mineral reaction:

$$Als + H_2O + CaO = Mrg$$

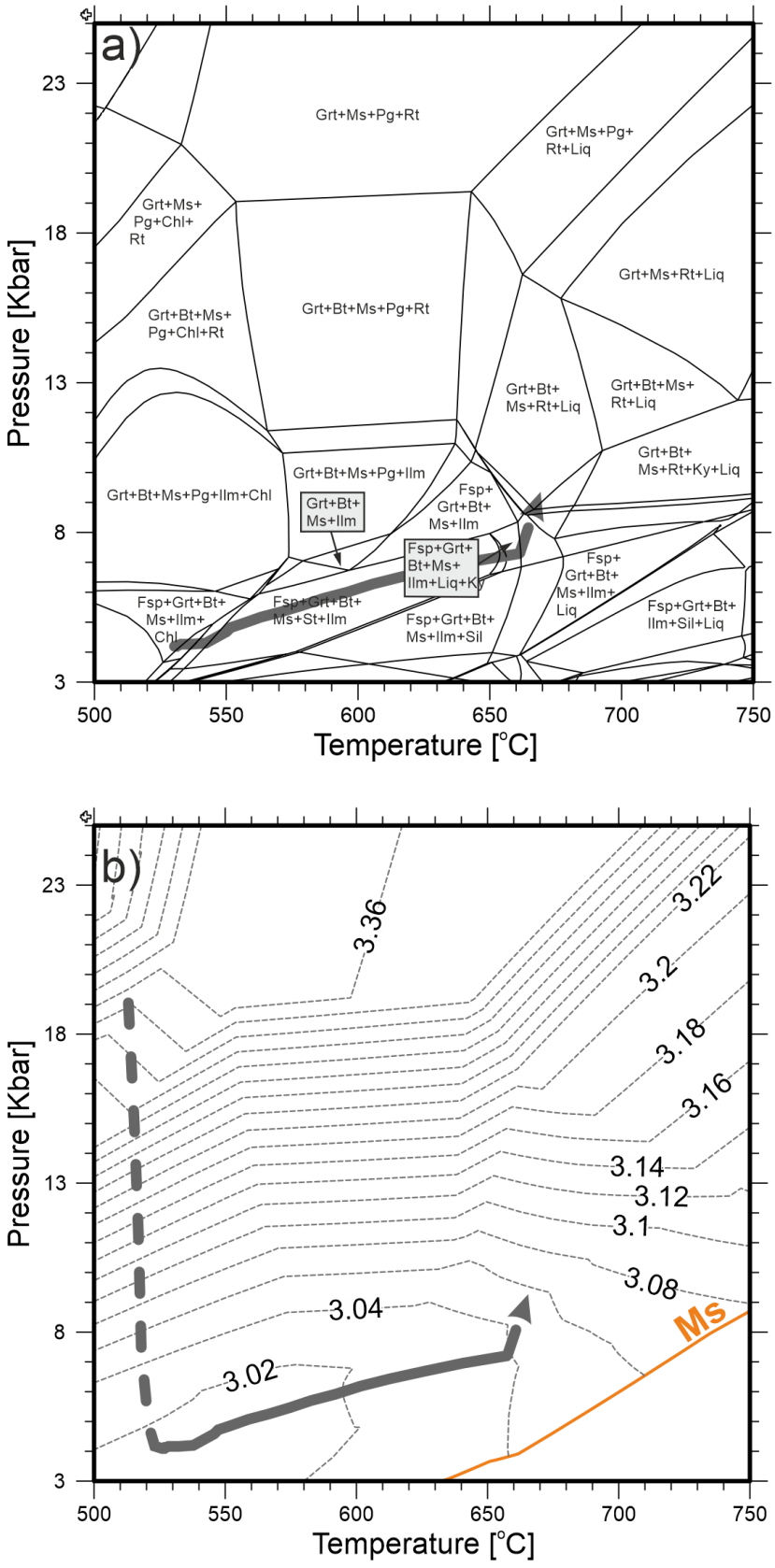

Fig. 34. Phase diagram modelling results for sample MD01-18 using the core composition of Grt and bulk rock composition; a. isochemical phase diagram, b. Compositional isopleths of Si in K- white mica. The stability field of white mica is additionally shown. Grey arrow on diagrams b and d is for the modelled P–T path.

It appears that the decomposition of Ca-bearing phases such as garnet or plagioclase may have served as a source of CaO for margarite formation according to the following simplified reactions (Baltatzis and Katagas, 1981):

$$Als + H_2O + Grs = Mrg + Qtz$$

$$Als + H_2O + An = Mrg + Qtz$$

The decomposition of anorthite and kyanite occurs in the P–T range of c. 538 to 575 and 5 to 7 kbar (Spear, 1993). Furthermore, margarite and quartz are low pressure products of the above reaction, consistent with our suggestion that margarite was produced on a retrograde path.

Sample MD01-02

The reconstructed P–T path for garnet composition of mica schist sample MD01-02 is shown in Fig. 35. Garnet growth modelling indicates that the garnet started to crystallize at 588°C and 8.3 kbar, and ceased at 662°C and 8.1 kbar within the stability field of garnet, plagioclase, biotite, K-white mica, ilmenite and melt (Fig. 35). Furthermore, garnet must have formed concurrently with low-Si white mica (c. 3.06 apfu, Fig. 35b). These minerals represent in fact the M2 mineral assemblage observed in the examined sample. Furthermore, the sample displays signs of incipient melting in agreement with thermodynamic calculations. On the other hand, this mica schist also contains several white mica plates with relatively high Si content, reaching up to 3.22 apfu (Fig. 33) and suggesting pressures of c. 11 to 18 kbar in the analysed temperature range based on compositional isopleths. However, considering that these high-Si white mica form core parts of the analysed flakes, we suggest that their formation preceded garnet crystallization. Considering the traces of only incipient melting observed in this sample, it seems that this part of the metamorphic history underwent in the temperatures lower than c. 570°C and pressures not exceeding c. 15 kbar. Higher temperatures and, consequently, higher pressures, according to the predictions of thermodynamic calculations, would result in an unexpectedly high volume of generated melt of even 25 vol%.

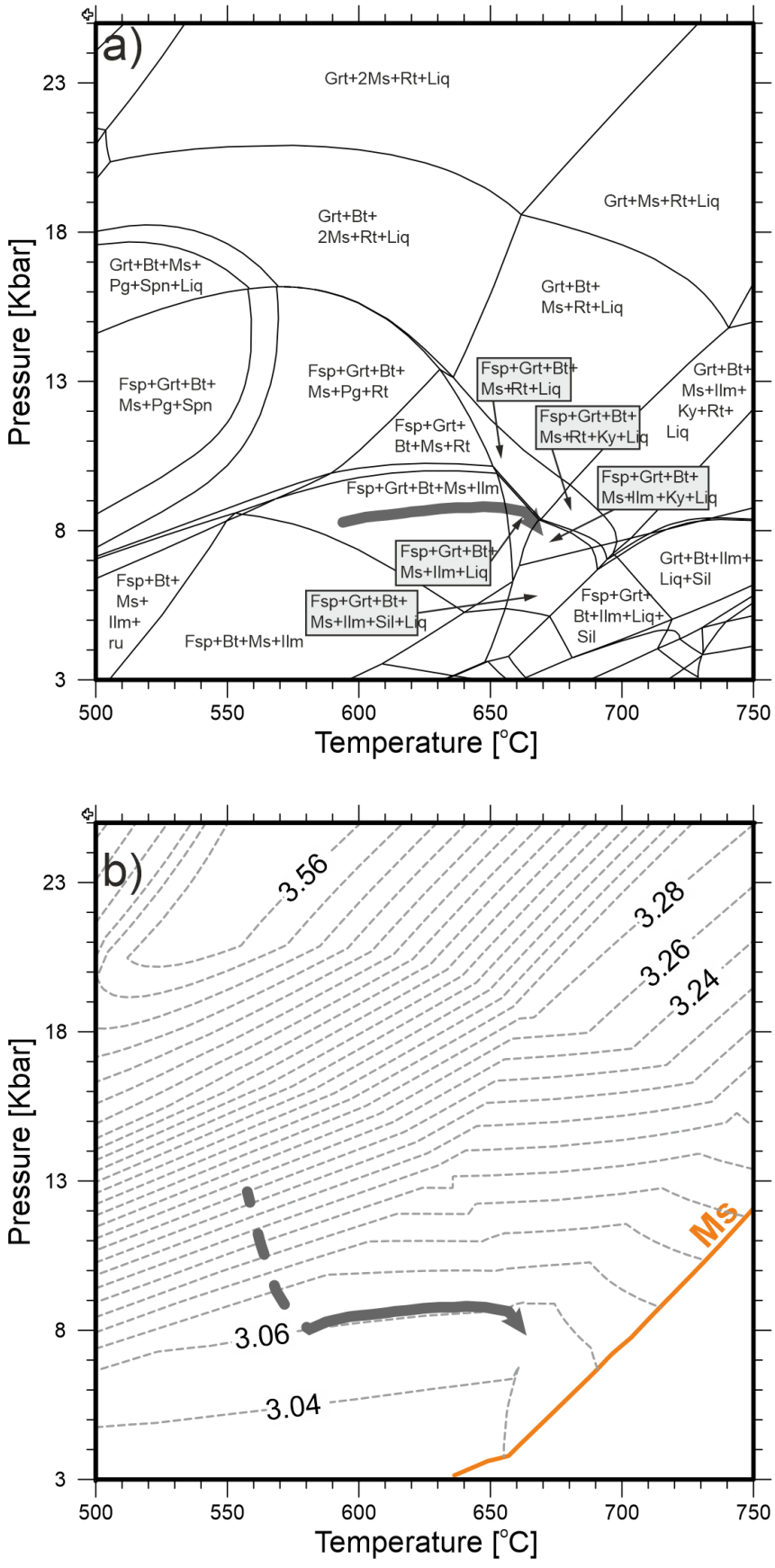

Fig. 35. Phase diagram modelling results for sample MD01-02 using the core composition of Grt and bulk rock composition; a. isochemical phase diagram, b. Compositional isopleths of Si in K- white mica. The stability field of white mica is additionally shown. Grey arrow on diagrams b and d is for the modelled P–T path.

Age of metamorphic events

Sample MD01-18 contained relatively large, up to 9 mm garnet crystals suitable for separate core and rim dating. Garnet cores, despite showing some scatter, define a decent quality, 345.3 ± 5.0 Ma Lu-Hf isochron (MSWD = 14) whereas garnet rims define only a rough age of 356± 40 Ma. The low precision of the latter age is associated with very low $^{176}Lu/^{177}Hf$ ratios (0.09-0.11) observed in garnet rims that are only slightly higher from the whole rock $^{176}Lu/^{177}Hf$ = 0.05. Additionally, we included all obtained data from core and rim into age calculations, which together with the whole rock define 346.9±3.6 Ma age (MSWD = 8.6). Similar to Lu-Hf analyses, Sm-Nd dating of garnet cores revealed excess scatter among the analysed fractions, which together with the whole rock define a poor quality age of 348 ± 17 Ma (MSWD = 55). Garnet rims together with the whole rock define 337.3 ± 6.6 Ma age (MSWD = 7.7).

Acknowledgements

We are grateful for the financial support provided by NCN research grants 2015/17/B/ST10/02212 (for JS, SI and RA) and 2018/29/B/ST10/01120 (for MJ). We would also like to thank Małgorzata Nowak for carefully reviewing the final version of the text.

References

Abati, J., Aghzer, A.M., Gerdes, A., Ennih, N., 2010. Detrital zircon ages of Neoproterozoic sequences of the Moroccan Anti-Atlas belt. Precambrian Research 181, 115–128. https://doi.org/10.1016/j.precamres.2010.05.018

Abdallah, N., Liégeois, J.-P., De Waele, B., Fezaa, N., Ouabadi, A., 2007. The Temaguessine Fe-cordierite orbicular granite (Central Hoggar, Algeria): U–Pb SHRIMP age, petrology, origin and geodynamical consequences for the late Pan-African magmatism of the Tuareg shield. Journal of African Earth Sciences 49, 153–178. https://doi.org/10.1016/j.jafrearsci.2007.08.005

Anderson, D.E., Buckley, G.R., 1973. Zoning in garnets?Diffusion models. Contr. Mineral. and Petrol. 40, 87–104. https://doi.org/10.1007/BF00378168

Armbruster, T., Bonazzi, P., Akasaka, M., Bermanec, V., Chopin, C., Gieré, R., Heuss-Assbichler, S., Liebscher, A., Menchetti, S., Pan, Y., Pasero, M., 2006. Recommended nomenclature of epidote-group minerals. European Journal of Mineralogy 18, 551–567. https://doi.org/10.1127/0935-1221/2006/0018-0551

Awdankiewicz, H., 2008. The petrology and geochemistryof the metabasites of the Niedzwiedz Massifin the Fore-Sudetic Block. Prace Państwowego Instytutu Geologicznego 189, 5–56.

Baltatzis, E., Katagas, C., 1981. Margarite pseudomorphs after kyanite in Glen Esk, Scotland. American Mineralogist 66, 213–216.

Bendaoud, A., Ouzegane, K., Godard, G., Liégeois, J.-P., Kienast, J.-R., Bruguier, O., Drareni, A., 2008. Geochronology and metamorphic P - T - X evolution of the Eburnean granulite-facies metapelites of Tidjenouine (Central Hoggar, Algeria): witness of the LATEA metacratonic evolution. Geological Society, London, Special Publications 297, 111–146. https://doi.org/10.1144/SP297.6

Bhatia, M.R., Crook, K.A.W., 1986. Trace element characteristics of graywackes and tectonic setting discrimination of sedimentary basins. Contributions to Mineralogy and Petrology 92, 181–193.

Bosch, D., Bruguier, O., Caby, R., Buscail, F., Hammor, D., 2016. Orogenic development of the Adrar des Iforas (Tuareg Shield, NE Mali): New geochemical and geochronological data and geodynamic implications. Journal of Geodynamics 96, 104–130. https://doi.org/10.1016/j.jog.2015.09.002

Buriánková, K., Hanžl, P., Mazur, S., Melichar, R., Leichmann, J., 1999. Geochemistry of the Doboszowice Orthogneisses and its Correlation with Rocks of the Silesicum and Moravicum. Geolines 8, 11.

Cao, W., Massonne, H.-J., Liang, X., 2021. Partial melting due to breakdown of phengite and amphibole in retrogressed eclogite of deep Precambrian crust: An example from the Algonquin terrane, western Grenville Province, Canada. Precambrian Research 352, 105965. https://doi.org/10.1016/j.precamres.2020.105965

Chatterjee, 1976. Margarite stability and compatibility relations in the system CaO-Al2O3-SiO2-H2O as a pressure-temperature indicator. American Mineralogist 61, 699–709.

Chopin, F., Schulmann, K., Skrzypek, E., Lehmann, J., Dujardin, J.R., Martelat, J.E., Lexa, O., Corsini, M., Edel, J.B., Štípská, P., Pitra, P., 2012. Crustal influx, indentation, ductile thinning and gravity redistribution in a continental wedge: Building a Moldanubian mantled gneiss dome with underthrust Saxothuringian material (European Variscan belt). Tectonics 31. https://doi.org/10.1029/2011TC002951

Collett, S., Schulmann, K., Deiller, P., Štípská, P., Peřestý, V., Ulrich, M., Jiang, Y., de Hoÿm de Marien, L., Míková, J., 2022. Reconstruction of the mid-Devonian HP-HT metamorphic event in the Bohemian Massif (European Variscan belt). Geoscience Frontiers 13, 101374. https://doi.org/10.1016/j.gsf.2022.101374

Collett, S., Štípská, P., Schulmann, K., Míková, J., Kröner, A., 2021. Tectonic significance of the Variscan suture between Brunovistulia and the Bohemian Massif. Journal of the Geological Society 178, jgs2020-176. https://doi.org/10.1144/jgs2020-176

Cullers, R.L., 2002. Implications of elemental concentrations for provenance, redox conditions, and metamorphic studies of shales and limestones near Pueblo, CO, USA. Chemical Geology 191, 305–327. https://doi.org/10.1016/S0009-2541(02)00133-X

Domeier, M., 2016. A plate tectonic scenario for the Iapetus and Rheic oceans. Gondwana Research 36, 275–295. https://doi.org/10.1016/j.gr.2015.08.003

Drost, K., Gerdes, A., Jeffries, T., Linnemann, U., Storey, C., 2011. Provenance of Neoproterozoic and early Paleozoic siliciclastic rocks of the Teplá-Barrandian unit (Bohemian Massif): Evidence from U–Pb detrital zircon ages. Gondwana Research 19, 213–231. https://doi.org/10.1016/j.gr.2010.05.003

Dziedzicowa, H., 1966. Seria łupków krystalicznych na wschód od strefy Niemczy w świetle nowych badań. The schists series east of the Niemcza Zone in the light of new investigations, (in Polish, English summary). Z geologii Ziem Zachod-nich 101–118.

Floyd, P.A., Winchester, J.A., Park, R.G., 1989. Geochemistry and tectonic setting of Lewisian clastic metasediments of the early Proterozoic Loch Maree Group of Gairloch, NW Scotland. Precambrian Res 45, 203–214.

Friedl, G., Finger, F., Paquette, J.-L., von Quadt, A., McNaughton, N.J., Fletcher, I.R., 2004. Pre-Variscan geological events in the Austrian part of the Bohemian Massif deduced from U-Pb zircon ages. International Journal of Earth Sciences 93, 802–823.

Gaucher, C., Finney, S., Poire, D., Valencia, V., Grove, M., Blanco, G., Pamoukaghlian, K., Peral, L., 2008. Detrital zircon ages of Neoproterozoic sedimentary successions in Uruguay and Argentina: Insights into the geological evolution of the Río de la Plata Craton. Precambrian Research 167, 150–170. https://doi.org/10.1016/j.precamres.2008.07.006

Geraldes, M.C., Nogueira, C., Vargas-Mattos, G., Matos, R., Teixeira, W., Valencia, V., Ruiz, J., 2014. U–Pb detrital zircon ages from the Aguapeí Group (Brazil): Implications for the geological evolution of the SW border of the Amazonian Craton. Precambrian Research 244, 306–316. https://doi.org/10.1016/j.precamres.2014.02.001

Gomez-Pugnaire, M.T., Visona, D., Franz, G., 1985. Kyanite, margarite and paragonite in pseudomorphs in amphibolitized eclogites from

the Betic Cordilleras, Spain. Chemical Geology 50, 129–141. https://doi.org/10.1016/0009-2541(85)90116-0

Green, T., Hellmann, P., 1982. Fe-Mg partitioning between coexisting garnet and phengite at high pressure, and comments on a garnetphengite geothermometer. Lithos 15, 253–266.

Henry, B., Liégeois, J.P., Nouar, O., Derder, M.E.M., Bayou, B., Bruguier, O., Ouabadi, A., Belhai, D., Amenna, M., Hemmi, A., Ayache, M., 2009. Repeated granitoid intrusions during the Neoproterozoic along the western boundary of the Saharan metacraton, Eastern Hoggar, Tuareg shield, Algeria: An AMS and U–Pb zircon age study. Tectonophysics 474, 417–434. https://doi.org/10.1016/j.tecto.2009.04.022

Hladil, J., Patocka, F., Kachlik, V., Melichar, R., Hubacik, M., 2003. Metamorphosed carbonates of Krkonose Mountains and Paleozoic evolution of Sudetic terranes (NE Bohemia, Czech Republic). GEOLOGICA CARPATHICA 54, 281–297.

Hynes, A., Forest, R.C., 1988. Empirical garnet-muscovite geothermometry in low-grade metapelites, Selwyn Range (Canadian Rockies). J Metamorph Geol 6, 297–309. https://doi.org/10.1111/j.1525-1314.1988.tb00422.x

Janoušek, V., Aichler, J., Hanžl, P., Gerdes, A., Erban, V., Žáček, V., Pecina, V., Pudilová, M., Hrdličková, K., Mixa, P., Žáčková, E., 2014. Constraining genesis and geotectonic setting of metavolcanic complexes: a multidisciplinary study of the Devonian Vrbno Group (Hrubý Jeseník Mts., Czech Republic). Int J Earth Sci (Geol Rundsch) 103, 455–483. https://doi.org/10.1007/s00531-013-0975-4

Jastrzębski, M., 2012. New insights into the polyphase evolution of the Variscan suture zone: evidence from the Staré Město Belt, NE Bohemian Massif. Geol. Mag. 149, 945–963. https://doi.org/10.1017/S0016756812000040

Jastrzębski, M., Budzyń, B., Stawikowski, W., 2017. Cambro-Ordovician vs Devono-Carboniferous geodynamic evolution of the Bohemian Massif: evidence from *P–T–t* studies in the Orlica–Śnieżnik Dome, SW Poland. Geological Magazine 156, 447–470. https://doi.org/10.1017/S0016756817000887

Jastrzębski, M., Machowiak, K., Krzemińska, E., Lang Farmer, G., Larionov, A.N., Murtezi, M., Majka, J., Sergeev, S., Ripley, E.M., Whitehouse, M., 2018. Geochronology, petrogenesis and geodynamic significance of the Visean igneous rocks in the Central Sudetes, northeastern Bohemian Massif. Lithos 316–317, 385–405. https://doi.org/10.1016/j.lithos.2018.07.034

Jastrzębski, M., Żelaźniewicz, A., Budzyń, B., Sláma, J., Konečny, P., 2020a. Age constraints on the Pre-Variscan and Variscan thermal events in the Kamieniec Ząbkowicki Metamorphic belt (the Fore-Sudetic Block, SW Poland). ASGP 90, 27–49. https://doi.org/10.14241/asgp.2020.05

Jastrzębski, M., Żelaźniewicz, A., Budzyń, B., Sláma, J., Konečny, P., 2020b. Age constraints on the Pre-Variscan and Variscan thermal events in the Kamieniec Ząbkowicki Metamorphic belt (the Fore-Sudetic Block, SW Poland). ASGP 90, 27–49. https://doi.org/10.14241/asgp.2020.05

Jastrzębski, M., Żelaźniewicz, A., Murtezi, M., Larionov, A.N., Sergeev, S., 2015. The Moldanubian Thrust Zone — A terrane boundary in the Central European Variscides refined based on lithostratigraphy and U–Pb zircon geochronology. Lithos 220–223, 116–132. https://doi.org/10.1016/j.lithos.2015.01.023

Jastrzębski, M., Żelaźniewicz, A., Stawikowski, W., Budzyń, B., Krzemińska, E., Machowiak, K., Madej, S., Białek, D., Sláma, J., Czupyt, Z., Jaźwa, A., 2023. The eastern part of the Saxothuringian Terrane characterized by zircon and monazite data from the Doboszowice Metamorphic Complex in the Sudetes (SW Poland). ASGP. https://doi.org/10.14241/asgp.2023.11

Jung, S., Masberg, P., Mihm, D., Hoernes, S., 2009. Partial melting of diverse crustal sources - Constraints from Sr-Nd-O isotope compositions of quartz diorite-granodiorite-leucogranite associations (Kaoko Belt, Namibia). Lithos 111, 236–251. https://doi.org/10.1016/j.lithos.2008.10.010

Kamzolkin, V.A., Ivanov, S.D., Konilov, A.N., 2016. Empirical phengite geobarometer: Background, calibration, and application. Geol. Ore Deposits 58, 613–622. https://doi.org/10.1134/S1075701516080092

Kohn, M.J., 2020. A refined zirconium-in-rutile thermometer. American Mineralogist 105, 963–971. https://doi.org/10.2138/AM-2020-7091/MACHINEREADABLECITATION/RIS

Kristoffersen, M., Andersen, T., Andresen, A., 2014. U–Pb age and Lu–Hf signatures of detrital zircon from Palaeozoic sandstones in the Oslo Rift, Norway. Geological Magazine 151, 816–829. https://doi.org/10.1017/S0016756813000885

Krogh, E.J., Raheim, A., 1978. Temperature and pressure dependence of Fe-Mg partitioning between garnet and phengite, with particular reference to eclogites. Contr. Mineral. and Petrol. 66, 75–80. https://doi.org/10.1007/BF00376087

Kröner, A., Hegner, E., 1998. Geochemistry, single zircon ages and Sm-Nd systematics of granitoid rocks from the Gory Sowie (Owl Mts), Polish west Sudetes: evidence for early Palaeozoic arc-related plutonism. J Geol Soc London 155, 711–724.

Kuznetsov, N.B., Meert, J.G., Romanyuk, T.V., 2014. Ages of detrital zircons (U/Pb, LA-ICP-MS) from the Latest Neoproterozoic–Middle Cambrian(?) Asha Group and Early Devonian Takaty Formation, the Southwestern Urals: A test of an Australia-Baltica connection within Rodinia. Precambrian Research 244, 288–305. https://doi.org/10.1016/j.precamres.2013.09.011

Mazur, S., Aleksandrowski, P., Kryza, R., Oberc-Dziedzic, T., 2006. The Variscan Orogen in Poland. GEOLOGICAL QUARTERLY 50, 89–118.

Mazur, S., Józefiak, D., 1999. Structural record of Variscan thrusting and subsequent extensional collapse in the mica schists from vicinities of Kamieniec Ząbkowicki, Sudetic foreland, SW Poland. Annales Societatis Geologorum Poloniae 69, 1–26.

Mazur, S., Kröner, A., Szczepański, J., Turniak, K., Hanžl, P., Melichar, R., Rodionov, N.V., Paderin, I., Sergeev, S.A., 2010. Single zircon U/Pb ages and geochemistry of granitoid gneisses from SW Poland: evidence for an Avalonian affinity of the Brunian microcontinent. Geol Mag 147, 508–526.

Mazur, S., Szczepański, J., Turniak, K., McNaughton, N.J., 2012. Location of the Rheic suture in the eastern Bohemian Massif: evidence from detrital zircon data. Terra Nova 24, 199–206. https://doi.org/10.1111/j.1365-3121.2011.01053.x

Mazur, S., Turniak, K., Szczepański, J., McNaughton, N.J., 2015. Vestiges of Saxothuringian crust in the Central Sudetes, Bohemian Massif: Zircon evidence of a recycled subducted slab provenance. Gondwana Research 27, 825–839. https://doi.org/10.1016/j.gr.2013.11.005

McLennan, S.M., Hemming, S., McDaniel, D.K., Hanson, G.N., 1993. Geochemical approaches to sedimentation, provenance, and tectonics. Special Paper - Geological Society of America 284, 21–40.

Meinhold, G., Morton, A.C., Fanning, C.M., Frei, D., Howard, J.P., Phillips, R.J., Strogen, D., Whitham, A.G., 2011. Evidence from detrital zircons for recycling of Mesoproterozoic and Neoproterozoic crust recorded in Paleozoic and Mesozoic sandstones of southern Libya. Earth and Planetary Science Letters 312, 164–175. https://doi.org/10.1016/j.epsl.2011.09.056

Moynihan, D.P., Pattison, D.R.M., 2013. An automated method for the calculation of *P-T* paths from garnet zoning, with application to metapelitic schist from the Kootenay Arc, British Columbia, Canada. Journal of Metamorphic Geology 31, 525–548. https://doi.org/10.1111/jmg.12032

Oberc-Dziedzic, T., Klimas, K., Kryza, R., Fanning, C., 2003. SHRIMP U-Pb zircon geochronology of the Strzelin gneiss, SW Poland: Evidence for a neoproterozoic thermal event in the Fore-Sudetic Block, Central European Variscides. INTERNATIONAL JOURNAL OF EARTH SCIENCES 92, 701–711.

Oberc-Dziedzic, T., Kryza, R., Madej, S., Pin, C., 2018. The Saxothuringian Terrane affinity of the metamorphic Stachów Complex (Strzelin Massif, Fore-Sudetic Block, Poland) inferred from zircon ages. Geological Quarterly 62. https://doi.org/10.7306/gq.1405

Oliver, G., Corfu, F., Krogh, T., 1993. U-Pb ages from SW Poland - evidence for a Caledonian suture zone between Baltica and Gondwana. J Geol Soc London 150, 355–369.

Orozbaev, R., Hirajima, T., Bakirov, Apas, Takasu, A., Maki, K., Yoshida, K., Sakiev, K., Bakirov, Azamat, Hirata, T., Tagiri, M., Togonbaeva, A., 2015. Trace element characteristics of clinozoisite pseudomorphs after lawsonite in talc-garnet-chloritoid schists from the Makbal UHP Complex, northern Kyrgyz Tian-Shan. Lithos 226, 98–115. https://doi.org/10.1016/j.lithos.2014.10.008

Pankhurst, R.J., Hervé, F., Fanning, C.M., Calderón, M., Niemeyer, H., Griem-Klee, S., Soto, F., 2016. The pre-Mesozoic rocks of northern Chile: U–Pb ages, and Hf and O isotopes. Earth-Science Reviews 152, 88–105. https://doi.org/10.1016/j.earscirev.2015.11.009

Parry, M., Štípská, P., Schulmann, K., Hrouda, F., Ježek, J., Kröner, A., 1997. Tonalite sill emplacement at an oblique plate boundary: northeastern margin of the Bohemian Massif. Tectonophysics 280, 61–81.

Peucat, J.J., Drareni, A., Latouche, L., Deloule, E., Vidal, P., 2003. U–Pb zircon (TIMS and SIMS) and Sm–Nd whole-rock geochronology of the Gour Oumelalen granulitic basement, Hoggar massif, Tuareg shield, Algeria. Journal of African Earth Sciences 37, 229–239. https://doi.org/10.1016/j.jafrearsci.2003.03.001

Pietranik, A., Majka, J., 2017. The Wilkow syenite – the unique remnant of the 380-360 Ma magmatic event at the Gondwana north-eastern margin. Mineralogia - Special Papers 47, 37.

Pietranik, A., Storey, C., Kierczak, J., 2013. The Niemcza diorites and moznodiorites (Sudetes, SW Poland): a record of changing geotectonic setting at ca. 340 Ma. Geological Quarterly 57. https://doi.org/10.7306/gq.1084

Puziewicz, J., Koepke, J., 2001. Partial melting of garnet-hornblende granofels and the crystallisation of igneous epidote in the Niedźwiedź Amphibolite Massif (Fore-Sudetic Block, SW Poland). Neues Jahrbuch für Mineralogie, Monatshefte 12, 529–547.

R Core Team, 2012. R: A language and environment for statistical computing. R Foundation for Statistical Computing.

Schulmann, K., Konopásek, J., Janousek, V., Lexa, O., Lardeaux, J.-M., Edel, J.-B., Stípská, P., Ulrich, S., 2009. An Andean type Palaeozoic convergence in the Bohemian Massif. Comptes Rendus Geosciences 341, 266–286.

Skacel, J., 1989. Crossing of the Lugian boundary fault with Nyznerov dislocation belt between Vapenna and Javornik in Silesia. Acta Universitatis Palackianae Olomucensis 95, 31–45.

Skrzypek, E., Lehmann, J., Szczepański, J., Anczkiewicz, R., Štípská, P., Schulmann, K., Kröner, A., Bia\lek, D., 2014. Time-scale of deformation and intertectonic phases revealed by P–T–D–t relationships in the orogenic middle crust of the Orlica-Śnieżnik Dome, Polish/Czech Central Sudetes. Journal of Metamorphic Geology 32, 981–1003.

Śliwiński, M., Jastrzębski, M., Sláma, J., 2022. Detrital zircon analysis of metasedimentary rocks of the Staré Mìsto Belt, Sudetes: implications for the provenance and evolution of the eastern margin of the Saxothuringian terrane, NE Bohemian Massif. Geological Quarterly 66, 1–21.

Spear, F.S., 1993. Metamorphic Phase Equilibria and Pressure-Temperature-Time Paths. Mineralogical Society of America 779.

Steltenpohl, M.G., Cymerman, Z., Krogh, E.J., Kunk, M.J., 1993. Exhumation of eclogitized continental basement during Variscan lithospheric delamination and gravitational collapse, Sudety Mountains, Poland. Geology 21, 1111–1114.

Štípska, P., Schulmann, K., Kröner, A., 2004. Vertical extrusion and middle crustal spreading of omphacite granulite: a model of syn-convergent exhumation (Bohemian Massif, Czech Republic). Journal of Metamorphic Geology 22, 179–198.

Szczepański, J., 2007. A vestige of an Early Devonian active continental margin in the East Sudetes (SW Poland) - evidence from geochemistry of the Jegłowa Beds, Strzelin Massif. Geological Quarterly 51, 271–284.

Szczepański, J, Anczkiewicz, R., Marciniak, D., 2022. P-T conditions and chronology of the Variscan collision in the easternmost part of the Saxothuringian crust. Mineralogia – Special Papers 50, 88.

Szczepański, J., Goleń, M., 2022. Tracing exhumation record in high-pressure micaschists: A new tectonometamorphic model of the evolution of the eastern part of the Fore Sudetic Block, Kamieniec Metamorphic Belt, NE Bohemian Massif, SW Poland. Geochemistry 82, 125859. https://doi.org/10.1016/j.chemer.2021.125859

Szczepański, J., Kaszuba, G., Anczkiewicz, R., Ilnicki, S., 2023a. Provenance of the early Palaeozoic volcano-sedimentary successions from eastern part of the Central Sudetes: implications for the tectonic evolution of the NE Bohemian Massif. Geol. Mag. 160, 1498–1534. https://doi.org/10.1017/S0016756823000523

Szczepański, J., Kaszuba, G., Anczkiewicz, R., Ilnicki, S., 2023b. Provenance of the early Palaeozoic volcano-sedimentary successions from eastern part of the Central Sudetes: implications for the tectonic evolution of the NE Bohemian Massif. Geological Magazine 1–37. https://doi.org/10.1017/S0016756823000523

Szczepański, J., Turniak, K., Anczkiewicz, R., Gleichner, P., 2020. Dating of detrital zircons and tracing the provenance of quartzites from the Bystrzyckie Mts: implications for the tectonic setting of the Early Palaeozoic sedimentary basin developed on the Gondwana margin. Int J Earth Sci (Geol Rundsch). https://doi.org/10.1007/s00531-020-01888-8

Szczepański, Jacek, Zhong, X., Dąbrowski, M., Wang, H., Goleń, M., 2022a. Combined phase diagram modelling and quartz-in-garnet barometry of *HP* metapelites from the Kamieniec Metamorphic Belt (NE Bohemian Massif). Journal Metamorphic Geology 40, 3–37. https://doi.org/10.1111/jmg.12608

Szczepański, Jacek, Zhong, X., Dąbrowski, M., Wang, H., Goleń, M., 2022b. Combined phase diagram modelling and quartz-in-garnet barometry of *HP* metapelites from the Kamieniec Metamorphic Belt (NE Bohemian Massif). Journal of Metamorphic Geology jmg.12608. https://doi.org/10.1111/jmg.12608

Tabaud, A.S., Štípská, P., Mazur, S., Schulmann, K., Míková, J., Wong, J., Sun, M., 2021. Evolution of a Cambro-Ordovician active margin in northern Gondwana: Geochemical and zircon geochronological evidence from the Góry Sowie metasedimentary rocks, Poland. Gondwana Research 90, 1–26. https://doi.org/10.1016/j.gr.2020.10.011

Taylor, S.R., McLennan, S.M., 1985. The Continental Crust: Its Composition and Evolution; An Examination of the Geochemical Record Preserved in Sedimentary Rocks. Blackwell Science Publications, Oxford.

Torsvik, T.H., 2017. Earth history and palaeogeography: Trond H. Torsvik, University of Oslo, and L. Robin M. Cocks, The Natural History Museum, London.

Tsujimori, T., Ernst, W.G., 2014. Lawsonite blueschists and lawsonite eclogites as proxies for palaeo-subduction zone processes: a review. Journal of Metamorphic Geology 32, 437–454. https://doi.org/10.1111/JMG.12057

Valley, J.W., 2003. Oxygen Isotopes in Zircon. Reviews in Mineralogy and Geochemistry 53, 343–385. https://doi.org/10.2113/0530343

Valverde-Vaquero, P., Dörr, W., Belka, Z., Franke, W., Wiszniewska, J., Schastok, J., 2000. U–Pb single-grain dating of detrital zircon in the Cambrian of central Poland: implications for Gondwana versus Baltica provenance studies. Earth and Planetary Science Letters 184, 225–240. https://doi.org/10.1016/S0012-821X(00)00312-5

Verma, S.P., Armstrong-Altrin, J.S., 2013. New multi-dimensional diagrams for tectonic discrimination of siliciclastic sediments and their application to Precambrian basins. Chemical Geology 355, 117–133. https://doi.org/10.1016/j.chemgeo.2013.07.014

Winchester, J.A., Floyd, P.A., 1977. Geochemical discrimination of different magma series and their differentiation products using immobile elements.

Chemical Geology 20, 325–343. https://doi.org/10.1016/0009-2541(77)90057-2

Wu, C.-M., Chen, H.-X., 2015. Calibration of a Ti-in-muscovite geothermometer for ilmenite- and Al2SiO5-bearing metapelites. Lithos 212–215, 122–127. https://doi.org/10.1016/j.lithos.2014.11.008

Žáčková, E., Konopásek, J., Košler, J., Jeřábek, P., 2010. Detrital zircon populations in quartzites of the Krkonoše–Jizera Massif: implications for pre-collisional history of the Saxothuringian Domain in the Bohemian Massif. Geological Magazine 149, 443–458. https://doi.org/10.1017/S0016756811000744

Žák, J., Sláma, J., 2018. How far did the Cadomian 'terranes' travel from Gondwana during early Palaeozoic? A critical reappraisal based on detrital zircon geochronology. International Geology Review 60, 319–338. https://doi.org/10.1080/00206814.2017.1334599

Zeng, L., Zhang, L., Yue, J., Li, X., 2019. Ultrahigh-pressure and high-P lawsonite eclogites in Muzhaerte, Chinese western Tianshan. Journal of Metamorphic Geology 37, 717–743. https://doi.org/10.1111/JMG.12482